FEATURE ARTICLE

Time-Dependent Quantum-Mechanical Methods for Molecular Dynamics

Ronnie Kosloff

Department of Physical Chemistry and The Fritz Haber Research Center for Molecular Dynamics, The Hebrew University, Jerusalem 91904, Israel (Received: December 7, 1987)

The basic framework of time-dependent quantum-mechanical methods for molecular dynamics calculations is described. The central problem addressed by computational methods is a discrete representation of phase space. In classical mechanics, phase space is represented by a set of points whereas in quantum mechanics it is represented by a discrete Hilbert space. The discretization described in this paper is based on collocation. Special cases of this method include the discrete variable representation (DVR) and the Fourier method. The Fourier method is able to represent a system in phase space with the efficiency of one sampling point per unit volume in phase space h, so that, with the proper choice of the initial wave function, exponential convergence is obtained in relation to the number of sampling points. The numerical efficiency of the Fourier method leads to the conclusion that computational effort scales semilinearly with the volume in the phase space occupied by the molecular system. Methods of time propagation are described for time-dependent and time-independent Hamiltonians. The time-independent approaches are based on a polynomial expansion of the evolution operator. Two of these approaches, the Chebychev propagation and the Lanczos recurrence, are also compared. Methods to obtain the Raman spectra directly by using the Chebychev propagation method are shown. For time-dependent problems unitary short-time propagators are described: the second-order differencing and the split operator. Consideration of all these methods has led to scaling laws of computation. The conclusion from such scaling laws is that, for simulations of complex molecular systems, approximation techniques have to be employed which reduce the dimensionality of the problem. The time-dependent self-consistent field (TDSCF) is suggested. Finally, a brief description is presented of current applications of the time-dependent method.

I. Introduction

Chemical change is brought about by the motion of electrons and nuclei within reacting molecules. The description of this internal motion is the subject of molecular dynamics. Theoretical advances in the field have been linked to the ability to calculate from first principles the basic molecular encounter. This paper is concerned with methods of calculation, particularly those of the solution of the time-dependent Schrödinger equation, applying the results to the numerical simulation of basic chemical events. The purpose of this paper is to set guidelines for constructing, as exactly as possible, calculations that are aimed at gaining detailed insight into the molecular system and that serve as benchmarks for other more approximate methods. All calculation methods scale in proportion to the volume of phase space that the molecular encounter occupies. Therefore, phase space is a common denominator by which different methods of calculation can be compared and the feasibility of the calculation estimated. One of the most important issues is the adaptability and flexibility of the method. Both these issues will be addressed by a description of the essential steps in time-dependent quantum-mechanical calculations.

In recent years molecular dynamics has been great strides.[1] The field has gone through a transition from indirect bulk-type experiments to direct experiments that study the elementary process without interference of secondary processes. This isolation of basic chemical encounters has motivated a theoretical interpretation based on first principles, i.e., the fundamental equations of motion.

Isolation of the elementary event can be achieved either in space or in time. For gas-phase encounters or gas–surface encounters isolation is achieved by high-vacuum techniques. The experiments are generally based on the seeded supersonic molecular beam.[2] In such an experiment molecules in the beam emerge at very low temperatures which enables control of the initial molecular state. With crossed-beam geometries, a direct study of bimolecular reactions is possible.[3-5] When the molecular beam is crossed with a laser beam, detailed studies of unimolecular dissociation can be made, in particular the dissociation of van der Waals molecules.[6-12] Colliding the beam with a solid surface allows the examination of basic gas–surface encounters.[13-26] For study of

(1) Levine, R. D.; Bernstein, R. B. *Molecular Reaction Dynamics and Chemical Reactivity*, 2nd ed.; Clarendon: Oxford, 1987.
(2) Kinsey, J. L. *Int. Rev. Sci. Phys. Chem.* **1972**, *9*, 173.
(3) Hershbach, D. R. *Adv. Chem. Phys.* **1966**, *10*, 319.
(4) Bernstein, R. B. *Adv. At. Mol. Phys.* **1979**, *15*, 167.
(5) Neumark, D. M.; Wodtke, A. M.; Robinson, G. N.; Hyden, C. C.; Shobatke, K.; Sparks, R. K.; Shafer, T. P.; Lee, Y. T. *J. Chem. Phys.* **1985**, *82*, 3067. Neumark, D. M.; Wodtke, A. M.; Robinson, G. N.; Hyden, C. C.; Lee, Y. T. *J. Chem. Phys.* **1985**, *82*, 3045.
(6) Smalley, R. E.; Wharton, L.; Levy, D. H.; Chandler, D. W. *J. Chem. Phys.* **1978**, *68*, 2487.
(7) Levy, D. H. *Annu. Rev. Phys. Chem.* **1980**, *31*, 197.
(8) Kommandeur, J. *Recl. Rev.* **1983**, *102*, 421.
(9) Beswick, J. A.; Jortner, J. *Adv. Chem. Phys.* **1981**, *47*, 363.
(10) Even, E. U.; Amirav, A.; Leutwyler, S.; Ondrechen, M. J.; Berkovitch-Yelin, Z.; Jortner, J. *Faraday Discuss. Chem. Soc.* **1982**, *73*, 153.
(11) McDonald, D. B.; Fleming, G. R.; Rice, S. A. *Chem. Phys.* **1981**, *60*, 335.
(12) McDonald, D. B.; Rice, S. A. *J. Chem. Phys.* **1981**, *74*, 4893.
(13) Toennies, J. P. In *Dynamics of Gas–Surface Interaction*; Benedek, G.; Valbusa, U., Eds.; Springer Verlag: Berlin, 1982; p 208.
(14) Barker, J. A.; Auerbach, D. J. *Surf. Sci. Rep.* **1984**, *4*, 1.
(15) Asscher, M.; Somorjai, G. A. In *Atomic and Molecular Beam Methods*, Scoles, G., Ed.; Oxford University Press: London, 1987.
(16) Poelsema, B.; de Zwart, S. T.; Comsa, G. *Phys. Rev. Lett.* **1982**, *49*, 578. Poelsema, B.; Palmer, R. L.; Comsa, G. *Surf. Sci.* **1984**, *136*, 1. Poelsema, B.; Verheij, L. K.; Comsa, G. *Faraday Discuss. Chem. Soc.* **1985**, *80*, 16.
(17) Poelsema, B.; Palmar, R. L.; Comsa, G. *Surf. Sci.* **1984**, *136*, 1.
(18) Poelsema, B.; Verheij, L. K.; Comsa, G. *Phys. Rev. Lett.* **1983**, *51*, 2410. Poelsema, B.; Comsa, G. *Faraday Discuss. Chem. Soc.* **1985**, *80*, 16.
(19) Goodman, F. O.; Wachman, H. Y. *Dynamics of Gas–Surface Scattering*; Academic: New York, 1976.
(20) Armand, G.; Manson, J. R. In *Dynamics on Surfaces—Proceedings of the 17th Jerusalem Symposium on Quantum Chemistry*; Pullman, B.; Jortner, J.; Nitzan, A.; Gerber, R. G., Eds.; Reidel: Dordrecht, Holland, 1984; p 59.

0022-3654/88/2092-2087$01.50/0 © 1988 American Chemical Society

elementary reactions in solution, spatial isolation is not possible. Recently developed new ultrafast laser pulses in the femtosecond regime allow a time isolation in which the elementary process can be studied before the surrounding solvent molecules can interfere.[27,28]

An important distinction exists between modeling and simulating a molecular system. The purpose of modeling is to gain insight into the mechanism of molecular phenomena. A simple calculation pointing to a possible theoretical interpretation is usually adequate. The aim of simulation is a quantitative comparison of theory to experiment. The possibility of simulation in molecular dynamics is the result of both the experimental isolation of phenomena and the rapid improvement in computers. In this present work, emphasis is on simulation methods, although the same theoretical tools can serve to construct models as well.

On the basis of first principles, there are four fundamental theoretical methods for describing and simulating the elementary dynamical event: (a) the classical trajectory method, (b) the semiclassical method, (c) the quantum coupled channel method, and (d) the quantum time-dependent method. These basic methods are also the foundation of the vast approximation techniques that have been developed in theoretical chemistry.

The working hypothesis in applying these methods to molecular dynamics simulations is the Born–Oppenheimer approximation which allows separation of the electronic from the nuclear motion.[29] The hypothesis leads to the potential energy surface on which the chemical event takes place. A generalization considering simultaneous motion on more than one potential energy surface is usually adequate for cases where the simple adiabatic Born–Oppenheimer approximation breaks down.[30]

The most widely used method is the classical trajectory approach.[31-33] In this treatment the motion of the nuclei on the Born–Oppenheimer potential surface is solved by using Newton's equations of motion. Once the potential energy surface is known, the method can be easily implemented. Starting from a known initial configuration, the interpretation of the results is simple. The method has been applied to a large number of systems describing isolated encounters. The classical trajectory method has been extended to processes in a condensed phase by using the generalized Langevin equation. It allows the description of systems in contact with a thermal bath.[34,35] Despite its success the classical trajectory method has major problems. A detailed classical trajectory simulation, with full final state resolution, requires extensive sampling in phase space which becomes extremely expensive in computation time. This drawback is especially significant when rare or slow chemical events are considered. Another shortcoming has been found for large molecular systems when the onset of chaos is reached at very low excitations, making the definition of normal modes impossible.[36] Nevertheless, these drawbacks are minor compared to the fact that the chemical motion is quantum mechanical in nature. Quantum effects, like tunneling or the influence of zero-point motion, are extremely important for basic chemical encounters[37] and represent an inherent obstacle to the trajectory approach which may lead to qualitatively different results.

Semiclassical methods aim to correct the flaws in the classical description by including the most important quantum effects, while maintaining the simple implementation of classical mechanics.[38-44] The rationale behind these methods is that because the nuclei are relatively heavy, quantum effects can be treated as corrections to the basically classical motion. The most developed semiclassical dynamical method is the Gaussian wave-packet approximation.[45-72] In this method the quantum wave packet is constrained to be of a Gaussian form. The Gaussian approximation method has been widely used in many applications with great success. Nevertheless, at this stage, the semiclassical method is a very delicate tool. Each system requires a special implementation, and the validity of the approximation is not known.

The main difficulty in exact quantum-mechanical calculations is their nonlocal character which means that a global simultaneous description of all the molecular phase space is required. The most mature quantum-mechanical approach is the stationary coupled channel approach (CC), which is based on a solution of the stationary scattering equation.[73] The method has been applied to

(21) Gibson, K. D.; Sibner, S. J., submitted for publication in *J. Chem. Phys.*
(22) Gibson, K. D.; Sibner, S. J. *Phys. Rev. Lett.* **1985**, *55*, 1514.
(23) Gibson, K. D.; Sibner, S. J. *Faraday Discuss. Chem. Soc.* **1985**, *80*, 203.
(24) Gibson, K. D.; Cerjan, C.; Light, J. C.; Sibner, S. J., submitted for publication in *J. Chem. Phys.*
(25) Hutson, J. M.; Schwartz, C. *J. Chem. Phys.* **1983**, *79*, 5179.
(26) Schwartz, C. *Phys. Rev. B: Condens. Matter* **1986**, *34*, 2834.
(27) Dantus, M.; Rosker, M. J.; Zewail, A. H. *J. Chem. Phys.* **1987**, *87*, 2395.
(28) Ruhman, S.; Joly, A. G.; Nelson, K. A. *J. Chem. Phys.* **1987**, *86*, 6563. Ruhman, S.; Williams, L. R.; Joly, A. G.; Kohler, K.; Nelson, K. A. *J. Chem. Phys.* **1987**, *91*, 2237.
(29) Balint Kurti, G. G. *Adv. Chem. Phys.* **1975**, *30*, 137.
(30) Nikitin, E. E.; Umanski, S. Ya. *Theory of Slow Atomic Collisions*; Springer Verlag: Berlin, 1984.
(31) Karplus, M.; Porter, R.; Sharma, R. D. *J. Chem. Phys.* **1965**, *49*, 3259. Doll, J. D. *Chem. Phys.* **1974**, *3*, 257.
(32) Truhlar, D. G.; Muckermanin, T. In *Physics of Atoms and Molecules*; Bernstein, R. B., Ed.; Plenum: New York, 1979.
(33) Porter, R. M.; Raff, L. M. In *Molecular Collisions*; Miller, W. H., Ed.; Plenum: New York, 1976.
(34) Adelman, S. A.; Doll, J. D. *J. Chem. Phys.* **1974**, *61*, 4242; *J. Chem. Phys.* **1976**, *64*, 2375; *J. Chem. Phys.* **1975**, *63*, 4906. Adelman, S. A. *Adv. Phys. Chem.* **1983**, *53*, 61.
(35) Tully, J. C. *Acc. Chem. Res.* **1981**, *14*, 188.
(36) Rolfe, T. J.; Rice, S. A. *J. Chem. Phys.* **1983**, *79*, 4863.
(37) *Proceedings of the 19th Jerusalem Symposium*; Pullman, B., Jortner, J., Eds.; Reidel: Dordrecht, Holland, 1986.
(38) Miller, W. H. *J. Chem. Phys.* **1971**, *54*, 5386.
(39) Miller, W. H. *Adv. Chem. Phys.* **1974**, *25*, 69.
(40) Miller, W. H. *Adv. Chem. Phys.* **1974**, *30*, 77.
(41) Doll, J. D. *Chem. Phys.* **1974**, *3*, 257.
(42) Doll, J. D. *J. Chem. Phys.* **1974**, *61*, 954.
(43) Masel, R. I.; Merril, R. P.; Miller, W. H. *J. Chem. Phys.* **1976**, *64*, 45.
(44) Masel, R. I.; Merril, R. P.; Miller, W. H. *Surf. Sci.* **1974**, *46*, 681.
(45) Heller, E. J. *J. Chem. Phys.* **1975**, *62*, 1544.
(46) Heller, E. J. *J. Chem. Phys.* **1976**, *65*, 1289.
(47) Heller, E. J. *J. Chem. Phys.* **1976**, *65*, 4979.
(48) Heller, E. J. *J. Chem. Phys.* **1977**, *67*, 3339.
(49) Heller, E. J. *J. Chem. Phys.* **1978**, *68*, 2066.
(50) Heller, E. J. *J. Chem. Phys.* **1978**, *68*, 3891.
(51) Heller, E. J. *J. Chem. Phys.* **1981**, *75*, 2923.
(52) Heller, E. J. *Acc. Chem. Res.* **1981**, *14*, 386.
(53) Kulander, K. C.; Heller, E. J. *J. Chem. Phys.* **1978**, *69*, 2439.
(54) Davis, M. J.; Heller, E. J. *J. Chem. Phys.* **1979**, *71*, 3383.
(55) Lee, S. Y.; Heller, E. J. *J. Chem. Phys.* **1979**, *71*, 4777.
(56) Brown, R. C.; Heller, E. J. *J. Chem. Phys.* **1981**, *75*, 186.
(57) Lee, S. Y.; Heller, E. J. *J. Chem. Phys.* **1982**, *76*, 3035.
(58) Tannor, D.; Heller, E. J. *J. Chem. Phys.* **1982**, *77*, 202.
(59) Heller, E. J.; Sundberg, R. L.; Tannor, D. *J. Chem. Phys.* **1982**, *86*, 1882.
(60) Blanco, M.; Heller, E. J. *J. Chem. Phys.* **1983**, *78*, 2504.
(61) Drolshagen, G.; Heller, E. J. *J. Chem. Phys.* **1983**, *79*, 2072.
(62) Drolshagen, G.; Heller, E. J. *Surf. Sci.* **1984**, *139*, 260.
(63) Drolshagen, G.; Heller, E. J. *Chem. Phys. Lett.* **1984**, *104*, 129.
(64) Drolshagen, G. *Comments At. Mol. Phys.* **1985**, *17*, 47.
(65) Weissman, Y.; Jortner, J. *J. Chem. Phys.* **1979**, *71*, 3880.
(66) Drolshagen, G.; Vollmer, R. *Chem. Phys. Lett.* **1985**, *122*, 333.
(67) Heather, R.; Metiu, H. *Chem. Phys. Lett.* **1985**, *118*, 558.
(68) Jackson, B.; Metiu, H. *J. Chem. Phys.* **1985**, *82*, 5707.
(69) Jackson, B.; Metiu, H. *J. Chem. Phys.* **1985**, *83*, 1952.
(70) Sawada, S.; Heather, R.; Jackson, B.; Metiu, H. *J. Chem. Phys.* **1985**, *83*, 3009.
(71) Sawada, S.; Metiu, H. *J. Chem. Phys.* **1986**, *84*, 227.
(72) Daniel, J.; Heller, E. *J. Chem. Phys.* **1987**, *87*, 5302.
(73) Levine, R. D. *Quantum Mechanics of Molecular Rate Processes*; Clarendon: Oxford, 1969.

many dynamical problems such as reactive scattering,[74-81] surface scattering,[24-26,82] and more. However, despite extensive effort invested into working out the approach, progess in simulating realistic systems has been slow. Only now, 10 years after the first reactive scattering result for the H + H_2 system, are results emerging for the isotopic analogue D + H_2.[83] The difficulty stems from the computational effort of the method, which scales as the number of channels cubed. Moreover, the method is difficult to implement primarily because it is a boundary-value problem which requires a special treatment for each system considered. For problems in which more than one continuum of final states exists in stimulated desorption (three continua), it is not clear how to apply the CC method.

The time-dependent quantum-mechanical methods are based on the solution of the time-dependent Schrödinger equation:[84-146]

$$i\hbar \frac{\partial \psi}{\partial t} = \hat{H}\psi \tag{1.1}$$

For many physical situations, time-dependent methods have their own advantages. Because they are initial value problems, the methods are easy to implement. This means also that only one column of the $\hat{S}$ matrix is calculated. In particular the time-dependent picture enables a simple treatment of continua and of the rearrangement problem in reactive scattering. Besides these technical advantages, time-dependent methods lead to a better interpretation of the physical mechanism under discussion. The time variable also enables a description of externally driven systems, by introducing time-dependent Hamiltonians. These systems include molecules subject to strong laser fields or in contact with stochastic baths.

Exact time-dependent methods were slow to develop. Initially they were obtained by expanding the state on a basis set, diagonalizing the Hamiltonian matrix in this set, and using the eigenvalues and eigenfunctions to propagate in time. The numerical cost of diagonalization scales as the number of expansion functions cubed ($O(N^3)$). Although diagonalization methods are possibly more efficient for small simple model problems, because of their fast computational scaling properties they have to be replaced for the simulation of realistic larger systems. This was the motivation for exploring new methods with slower scaling properties. The first departure from the fast scaling limitation was introduced in the work of McCullough and Wyatt,[84] who used a finite difference scheme combined with an implicit propagator. The method scales as $O(N^2)$, where N is the number of grid points (spatial points used to represent the system). The finite difference has been improved by Askar using the explicit second-order-differencing propagator[85] where the method scales as $O(N)$. The slow con-

(74) Johnson, R. B. In *Algorithms and Computer Codes for Atomic and Molecular Quantum Scattering Theory*; Thomas, L., Ed.; National Resource for Computation in Chemistry Proceedings, No. 5; 1979; Vol. 1, p 86.

(75) Parker, G. A.; Shmaltz, T. G.; Light, J. C. In *Algorithms and Computer Codes for Atomic and Molecular Quantum Scattering Theory*; Thomas, L., Ed.; National Resource for Computation in Chemistry Proceedings, No. 5; 1979; Vol. 1, p 172.

(76) Light, J. C. *Discuss. Faraday Soc.* **1969**, *44*, 14.

(77) Wagner, W. A. *J. Chem. Phys.* **1970**, *65*, 4343.

(78) Wolken, G. *J. Chem. Phys.* **1973**, *58*, 3047.

(79) Chow, H.; Thompson, E. D. *Surf. Sci.* **1976**, *59*, 225.

(80) Schatz, G. C.; Kuppermann, A. *J. Chem. Phys.* **1976**, *65*, 4668.

(81) Redmon, M. J.; Wyatt, R. E. *Chem. Phys. Lett.* **1979**, *63*, 209. McNutt, J. F.; Wyatt, R. E.; Redmon, M. J. *J. Chem. Phys.* **1984**, *81*, 1692.

(82) Yu, C.; Whaley, K. B.; Hogg, C. S.; Sibener, S. *Phys. Rev. Lett.* **1983**, *51*, 2210.

(83) Webster, F.; Light, J. C. *J. Chem. Phys.* **1986**, *85*, 4744.

(84) McCullough, E. A.; Wyatt, R. E. *J. Chem. Phys.* **1969**, *51*, 1253; *J. Chem. Phys.* **1971**, *54*, 3592.

(85) Askar, A.; Cakmak, A. S. *J. Chem. Phys.* **1978**, *68*, 2794.

(86) Smith, C. B.; Raff, L. M.; Agrawal, P. M. *J. Chem. Phys.* **1985**, *83*, 1411. Agrawal, P. M.; Raff, L. M. *J. Chem. Phys.* **1982**, *77*, 3946.

(87) Kulander, K. C. *J. Chem. Phys.* **1978**, *69*, 5064.

(88) Gray, J. C.; Fraser, G. A.; Truhlar, D. G.; Kulander, K. C. *J. Chem. Phys.* **1980**, *73*, 5726.

(89) LeForestier, C.; Bergeron, G.; Hiberty, P. C. *Chem. Phys. Lett.* **1981**, *84*, 385.

(90) LeForestier, C. *Chem. Phys.* **1984**, *87*, 241.

(91) Kulander, K. C.; Sandhya Devi, K. R.; Koonin, S. E. *Phys. Rev. A* **1982**, *25*, 2982.

(92) Bergeron, G.; Hiberty, P. C.; LeForestier, C. *Chem. Phys.* **1985**, *93*, 253.

(93) Christoffel, K. M.; Brumer, P. *Phys. Rev. A* **1986**, *33*, 1309.

(94) Kosloff, D.; Kosloff, R. *J. Comput. Phys.* **1983**, *52*, 35.

(95) Kosloff, R.; Kosloff, D. *J. Chem. Phys.* **1983**, *79*, 1823.

(96) Yinnon, A. T.; Kosloff, R. *Chem. Phys. Lett.* **1983**, *102*, 216.

(97) Gerber, R. G.; Yinnon, A. T.; Kosloff, R. *Chem. Phys. Lett.* **1984**, *105*, 523.

(98) Gerber, R. B.; Yinnon, A. T.; Kosloff, R. *Chem. Phys.* **1984**, *87*, 441.

(99) Tal-Ezer, H.; Kosloff, R. *J. Chem. Phys.* **1984**, *81*, 3967.

(100) Bisseling, R. H.; Kosloff, R. *J. Comput. Phys.* **1985**, *59*, 136.

(101) Kosloff, R.; Cerjan, C. *J. Chem. Phys.* **1984**, *81*, 3722.

(102) Yinnon, A. T.; Kosloff, R.; Gerber, R. B. *Surf. Sci.* **1984**, *148*, 148.

(103) Bisseling, R. H.; Kosloff, R.; Manz, J. *J. Chem. Phys.* **1985**, *83*, 993.

(104) Bisseling, R. H.; Kosloff, R.; Manz, J.; Schor, H. H. R. *Ber. Bunsen-Ges. Phys. Chem.* **1985**, *89*, 270.

(105) Benjamin, I.; Bisseling, R. H.; Kosloff, R.; Levine, R. D.; Manz, J.; Schor, H. H. R. *Chem. Phys. Lett.* **1985**, *116*, 255.

(106) Kosloff, R.; Tal-Ezer, H. *Chem. Phys. Lett.* **1986**, *127*, 223.

(107) Cerjan, C.; Kosloff, R. *Phys. Rev. B: Condens. Matter* **1986**, *34*, 3832.

(108) Gerber, R. B.; Kosloff, R.; Berman, M. *Comput. Phys. Rep.* **1986**, *5*, 59.

(109) Bisseling, R. H.; Kosloff, R.; Manz, J.; Mrugala, F.; Romelt, J.; Weichselbaumer, G. *J. Chem. Phys.* **1986**, *86*, 2626.

(110) Tannor, D.; Kosloff, R.; Rice, S. *J. Chem. Phys.* **1986**, *85*, 5805.

(111) Rice, S. A.; Tannor, D. J.; Kosloff, R. *J. Chem. Soc., Faraday Trans. 2* **1986**, *82*, 2423.

(112) Cerjan, C.; Kosloff, R. *J. Phys. B* **1987**, *20*, 4441.

(113) Bisseling, R. H.; Kosloff, R. *J. Comput. Phys.*, in press.

(114) Kosloff, R.; Hammerich, A. D.; Ratner, M. A. In *Large Finite Systems*; *20th Jerusalem Symposium*; Jortner, J., Pullman, A., Pullman, B., Eds.; Reidel: Dordrecht, Holland, 1987; p 53.

(115) Bisseling, R. H.; Kosloff, R.; Gerber, R. B.; Ratner, M. A.; Gibson, L.; Cerjan, C. *J. Chem. Phys.* **1987**, *87*, 2760.

(116) Drolshagen, G.; Vollmer, R. *Chem. Phys. Lett.* **1985**, *122*, 333.

(117) Feit, M. D.; Fleck, J. A., Jr.; Steiger, A. *J. Comput. Phys.* **1982**, *47*, 412.

(118) Feit, M. D.; Fleck, J. A. *J. Chem. Phys.* **1982**, *78*, 301.

(119) Feit, M. D.; Fleck, J. A. *J. Chem. Phys.* **1984**, *80*, 2578.

(120) Yevick, D.; Hermansson, B. *J. Phys. C* **1985**, *18*, 4303.

(121) Yevick, D.; Hermansson, B. *Solid State Commun.* **1985**, *54*, 197.

(122) Mowrey, R. C.; Kouri, D. *Chem. Phys. Lett.* **1985**, *119*, 285. Mowrey, R. C.; Kouri, D. J. *J. Chem. Phys.* **1986**, *84*, 6466.

(123) Kouri, D. J.; Mowrey, R. C. *J. Chem. Phys.* **1987**, *86*, 2087.

(124) Mowrey, R. C.; Brown, H. F.; Kouri, D. J. *J. Chem. Phys.* **1987**, *86*, 2441.

(125) Mowrey, R. C.; Kouri, D. J. *J. Chem. Phys.* **1987**, *86*, 6140.

(126) Mowrey, R. C.; Kouri, D. J. *J. Chem. Phys.*, in press.

(127) Sun, Y.; Mowrey, R. C.; Kouri, D. J. *J. Chem. Phys.* **1987**, *87*, 339.

(128) Zhang, Z. H.; Kouri, D. H. *Phys. Rev. A* **1986**, *34*, 2687.

(129) Gray, S. K. *J. Chem. Phys.* **1987**, *87*, 2051.

(130) Mohan, V.; Sathyamurthy, N. *Curr. Sci.* **1986**, *55*, 115.

(131) Kono, H.; Lin, S. H. *J. Chem. Phys.* **1986**, *84*, 1071.

(132) Hellsing, B.; Nitzan, A.; Metiu, H. *Chem. Phys. Lett.* **1986**, *123*, 523.

(133) Wahnstrom, G.; Metiu, H. *Chem. Phys. Lett.* **1987**, *134*, 531.

(134) Jackson, B.; Metiu, H. *J. Chem. Phys.* **1987**, *86*, 1026.

(135) Heather, R.; Metiu, H. *J. Chem. Phys.* **1987**, *86*, 5009.

(136) Chiang, C. M.; Jackson, B. *J. Chem. Phys.* **1987**, *87*, 5497.

(137) Jackson, B. *J. Chem. Phys.*, in press.

(138) Joseph, T.; Kruel, T. M.; Manz, J.; Rexrodt, I. *Chem. Phys.* **1987**, *113*, 113.

(139) Joseph, T.; Manz, J. *Mol. Phys.* **1986**, *58*, 1149.

(140) Huber, D.; Heller, E. *J. Chem. Phys.* **1987**, *87*, 5302.

(141) Halcomb, L. L.; Diestler, D. J. *J. Chem. Phys.* **1986**, *84*, 3130.

(142) Selloni, A.; Car, R.; Parrinello, M.; Carnevali, P. *J. Phys. Chem.* **1987**, *91*, 4947.

(143) Selloni, A.; Carnavali, P.; Car, R.; Parrinello, M. *Phys. Rev. Lett.* **1987**, *59*, 823.

(144) Park, T. J.; Light, J. C. *J. Chem. Phys.* **1986**, *85*, 5870.

(145) Kottler, Z.; Nitzan, A.; Kosloff, R. In *Proceedings of the 19th Jerusalem Symposium*; Pullman, B., Jortner, J. Eds.; Reidel: Dordrecht, Holland, 1986.

(146) Nitzan, A.; Landmann, U., to be published.

vergence rate with respect to grid size of finite differencing limits its use to only qualitative problems.

The introduction of the Fourier method[94,117] has solved the problem of accuracy. The results of the calculation converge exponentially with respect to grid size. The method is also extremely efficient due to the fast Fourier transform (FFT) algorithm, which scales as $O(N \log N)$.[147-149] Moreover, with the use of modern computer architecture the scaling can be reduced to $O(\log N)$.[150] The accuracy and efficiency of the Fourier method have made it a leading example by which other calculational methods can be compared.

The present paper concentrates on exact time-dependent quantum-mechanical methods. Approximate semiclassical time-dependent methods which have been extensively studied by Heller and co-workers[45-72] will not be described here. The main considerations leading to the development of exact time-dependent methods are presented. Details are described when they have importance for the general picture or when they have not been published previously such as the calculation of a spectrum using the Chebychev propagator. Rather than give a complete review, the emphasis is on general principles and on the relationship to other methods of calculation. Special attention is given to the construction of computational scaling laws. Extrapolating on the present extremely rapid growth of the field, it is expected that time-dependent quantum-mechanical methods will become an everyday tool in physical chemistry of both the experimentalist and the theorist. This work is aimed therefore at opening the "black box" of the method and to shed light on the main design considerations. With this knowledge the casual user can understand the limitations and cost of using the "black box" of time-dependent quantum-mechanical calculational methods.

The implementation of the time-dependent method can be divided into five steps: (a) representation; (b) initiation; (c) Hamiltonian operation; (d) time propagation; (e) analysis of results. Section II is devoted to the description of steps a–c. Section III describes steps d and e. Section IV deals with current applications and the TDSCF approximation, and section V is an overview.

II. Representation

II.1. Phase Space and Hilbert Space. Our understanding of physical phenomena relies heavily on the idea of continuity. In particular the laws of mechanics are defined by continuous functions. The idea that local properties of a continuous function determine its global character is the source of the well-known perturbation approach. The same concept is the basis of the computational approaches in which a continuous function can be completely represented by a set of sampling points. A numerical approach is consequently dominated by the rate of convergence of an approximation based on a finite set of sampling points. The efficiency of a computational scheme can be judged by the convergence speed with respect to the number of representation values.

In molecular dynamics two fundamental concepts have to be represented: the state of the system and the operators that represent observables of the system. There is a significant difference in the way molecular dynamics is represented in classical and in quantum mechanics, phase space being the common denominator to which a comparison can be made.

In classical mechanics a point in phase space represents the state of the dynamical system.[151] A trajectory originating from this point describes the evolutionary dynamics of the system through time. The evolution is a manifestation of the classical equations of motion and of the initial conditions. Knowledge of position and momentum is required for all degrees of freedom. The local point representation in phase space is the reason why the classical trajectory method in molecular dynamics is easily implemented. Despite its advantage, however, the point representation in phase space is a source of a major difficulty. Even not considering the uncertainty relation, a strict point localization of a system in phase space is not possible. In practical terms a system has to be localized. This means that the trajectory must represent a bundle of neighboring trajectories in order to faithfully portray the true dynamics. The stability of this bundle of trajectories has been the subject of research effort for many years.[152] For integrable classical systems, stability is assured by the KAM theorem,[153] but most large molecular systems are not integrable. The onset of chaos even appears at energies that include only the zero-point motion in the molecular vibrational modes. Under such conditions neighboring trajectories diverge and all stability is lost.

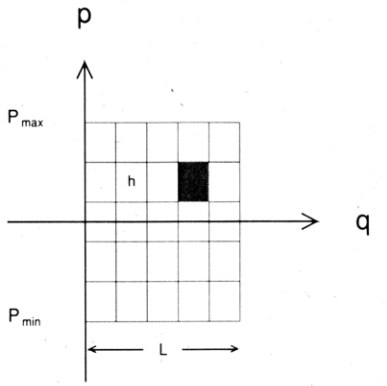

Figure 1. Rectangular-shaped phase space. The extent in coordinate space is L, and the extent in momentum space is $2P_{max}$. One unit cell is darkened. The volume of this phase space is $25h$; therefore the number of grid points $N = 25$, $\Delta x = L/N = h/2P_{max}$, and $\Delta p = h/\Delta x$.

In quantum mechanics, the minimum volume in which a physical system can be localized in phase space is h^D (h is Planck's constant and D the number of degrees of freedom). This means that a discrete representation is possible with at least one point per unit volume $h.^D$. The fundamental nonlocal character of a quantum-mechanical system poses the problem that the dynamics of a system cannot be confined to a finite volume in phase space; only its lower bound can be ascertained, the minimum value h^D. This is the main source of error in finite approximation of a quantum system.

To summarize, in classical mechanics the local character enables the motion to be confined within an upper boundary surface in phase space. The difficulty arises because of the use of a local representation in which a single point is not always an adequate representation of a small neighboring volume in phase space. In quantum mechanics, on the other hand, a strict lower boundary is set by the minimum localization volume h^D. An upper boundary surface in phase space cannot be strictly defined because of the nonlocal character of the theory.

The finite representation of phase space in quantum mechanics is the basis of the computational methods used to solve the quantum-mechanical equations of motion. The shape of the unit volume element is arbitrary. This fact can be utilized to optimize the representation for a particular problem. Figure 1 displays a rectangular-shaped unit volume used in the Fourier method described below.

The construction of a quantum-mechanical representation of phase space is closely connected to the representation of the wave function in Hilbert space. In the next section the possibility of accurately representing phase space in quantum mechanics with one point per unit volume will be demonstrated.

(147) Cooley, J. W.; Tukey, J. W. *Math. Comput.* **1965**, *19*, 297.
(148) Temperton, C. *J. Comput. Phys.* **1983**, *52*, 1.
(149) Nussbaumer, H. J. *Fast Fourier Transform and Convolution Algorithms*, 2nd ed.; Springer Verlag: Berlin, 1982.
(150) Swarztrauber, P. N. In *Parallel Computations*; Rodrigue, G., Ed.; Academic: New York, 1982.
(151) Percival, I.; Richards, D. *Dynamics*; Cambridge University Press: Cambridge, 1982.
(152) See, for example, the set of papers in *Topics in Nonlinear Dynamics*; Jorna, S., Ed.; AIP Conference Proceedings 46; American Institute of Physics: New York, 1978; 403.
(153) Arnold, W. I.; Avez, A. *Ergodic Problems of Classical Mechanics*; Benjamin: New York, 1974.

II.2. Representation in Hilbert Space. The nonlocal character of quantum mechanics must be overcome in constructing a representation. The use of Hilbert space is the method for solving this difficulty because it enables the description of nonlocal operators. The structure of the Hilbert space determines the representation in phase space, an issue that will be addressed later in this section. For a calculation scheme the Hilbert space must be discrete. Out of many alternatives the collocation method due to Gauss has been chosen by this author, for the construction of the discrete Hilbert space. The next section will review the basic features of the collocation method.

Consider approximating an arbitrary function $f(x)$ by a set of functions $g_n(x)$:

$$f(x) \approx \sum_{n=0}^{N-1} a_n g_n(x) \tag{2.1}$$

The question is how to determine the expansion coefficients a_n. In the collocation method these expansion coefficients are determined by matching the solution on a set of N grid points:

$$f(x_j) = \sum_{n=0}^{N-1} a_n g_n(x_j) \tag{2.2}$$

where x_j are the grid points (or collocation points). This equation is equivalent to a set of coupled linear equations. In matrix form they become

$$\mathbf{f} = \tilde{\mathbf{G}}\mathbf{a} \tag{2.3}$$

where $f_j = f(x_j)$ and $\tilde{G}_{nj} = g_n(x_j)$, which has a solution provided $g_n(x_j)$ are linearly independent:

$$\mathbf{a} = \tilde{\mathbf{G}}^{-1}\mathbf{f} \tag{2.4}$$

The functional basis that is connected through the expansion coefficients to the spatial grid allows the accurate representation of nonlocal operators. For example, the momentum operator $-i\hbar(\partial/\partial x)$ operating on a grid point j becomes

$$-i\hbar \frac{\partial}{\partial x} f(x_j) \approx -i\hbar \sum_{n=0}^{N-1} a_n \frac{\partial}{\partial x} g_n(x_j) \tag{2.5}$$

The choice of the functions $g_n(x)$ and the sampling points x_j has great influence on the quality of the approximation. Boundary conditions can be matched by choosing $g_n(x)$ to satisfy the boundary conditions.

A great simplification is achieved if the set $g_n(x)$ is chosen from an orthogonal base. One approach is to use quadrature points of orthogonal polynomials:

$$g_n(x) = w(x)p_n(x) \tag{2.6}$$

where $w(x)$ is a weight function and $p_n(x)$ is an orthogonal polynomial. The sampling points are chosen as zeros of $p_N(x)$. The theory of Gaussian integration then assures that the vectors $\boldsymbol{g}_n$ are orthogonal. The orthogonality can be used to solve (2.4):

$$a_n = \sum_{j=1}^{N} f(x_j)g_n(x_j) \tag{2.7}$$

It has been shown by Schwartz[154] that (2.1) is completely equivalent to

$$f(x) \approx \sum_{j=1}^{N} \frac{f(x_j)g_N(x)}{(x - x_j)g_N'(x_j)} \tag{2.8}$$

where the sampling points x_j are zeros of $g_N(x)$ and g_N can be any continuous function with N zeros. This formula can be used as a basis for calculating derivatives on the grid points. The use of this formula scales as $O(N^2)$ for N derivatives on all grid points. This can be improved by using the partial summation method of Lanczos[155] to obtain scaling as $O(N)$. Part of these ideas are well discussed in the work of Gottlieb and Orszag[156] and are known as the pseudospectral method. In molecular dynamics the same approach is known through the work of J. C. Light and co-workers as the *d*iscrete *v*ariable *r*epresentation (DVR).[157,158]

Examining the scaling of a numerical effort in calculating nonlocal operators, the linear relations (2.3) and (2.4) mean that this effort scales as $O(N^2)$. If the total number of representation points is proportional to the volume of phase space containing the system, the numerical effort will scale as this volume squared.

II.3. The Fourier Method. The Fourier method is a special case of an orthogonal collocation representation. This method deserves special attention for two reasons: first, it can be shown that the limit of one point per unit volume in phase space can be approached. Second, because it has great numerical advantages. Due to the FFT algorithm,[147-150] numerical effort scales semilinearly with the volume of phase space.

In the Fourier method the orthogonal functions $g_n(x)$ are chosen as

$$g_k(x) = e^{i2\pi kx/L}, \quad k = -(N/2 - 1), ..., 0, ..., N/2 \tag{2.9}$$

and the sampling points are equally spaced: $x_j = (j - 1)\Delta x$ and $\boldsymbol{L}$ is the length of the interval. With this choice a wave function $\psi(x)$ is represented as

$$\psi(x) \approx \sum_{k=-(N/2-1)}^{N/2} a_k e^{i2\pi kx/L} \tag{2.10}$$

The expansion coefficients a_k become the Fourier expansion coefficients. The choice of the expansion functions (2.9) implies periodic boundary conditions with period $\boldsymbol{L}$. One can use the orthogonality of the Fourier functions with equidistant sampling points to invert the relation, giving

$$a_k = \frac{1}{N}\sum_{j=1}^{N} \psi(x_j)e^{-i2\pi kx_j/L} \tag{2.11}$$

In quantum mechanics the coefficients a_k have an important interpretation since they represent the amplitude of the wave function in momentum space.

At this point the phase-space representation should be reconsidered. The minimum volume in phase space covered by the Fourier representation is calculated as follows: The length of the spatial dimension in phase space is $\boldsymbol{L}$ and the maximum momentum is $\boldsymbol{p}_{max}$. Therefore, the represented volume becomes Vol $= 2\boldsymbol{L}\cdot\boldsymbol{p}_{max}$, where the factor of 2 appears because the momentum range is from $-\boldsymbol{p}_{max}$ to $+\boldsymbol{p}_{max}$. By use of the fact that $\boldsymbol{p} = \hbar\boldsymbol{k}$, the phase-space volume can be expressed

$$\text{Vol} = 2\hbar\boldsymbol{L}\cdot\boldsymbol{k}_{max} = Nh \tag{2.12}$$

where N is the number of sampling points. Then the sampling spacing Δx is related to the maximum wave vector via

$$\Delta x = \pi/|\boldsymbol{k}_{max}| \tag{2.13}$$

Figure 1 expresses the relation between the volume in phase space, the unit volume, and the grid parameters Δx and N. The computational scaling properties of the Fourier method are a result of the scaling properties of the FFT algorithm, which scales as $O(N \log N)$.[147] As a result, the Fourier method scales with phase space as $O((\text{Vol}) \log (\text{Vol}))$.

A function that is bounded in momentum space is equivalent to the Fourier transform of the function being band limited. Confinement of such a function to a finite volume in phase space is equivalent to a band limited function with finite support. The accuracy of a representation of this function is assured by the Whittaker–Kotel'nikov–Shannon sampling theorem.[159-161] It states that a band-limited function with finite support is fully specified if the functional values are given by a discrete, sufficiently dense set of equally spaced sampling points. The number of points

(154) Schwartz, C. *J. Math. Phys.* **1985**, *26*, 411.
(155) Lanczos, C. *Applied Analysis*; Prentice-Hall: Englewood Cliffs, NJ, 1956.
(156) Gottlieb, D.; Orszag, S. A. *Numerical Analysis of Spectral Methods: Theory and Applications*; SIAM: Philadelphia, 1977.
(157) Lill, J. V.; Parker, G. A.; Light, J. C. *Chem. Phys. Lett.* **1982**, *89*, 483. Light, J. C.; Hamilton, I. P.; Lill, J. V. *J. Chem. Phys.* **1985**, *82*, 1400.
(158) Hamilton, J. P.; Light, J. C. *J. Chem. Phys.* **1986**, *84*, 306.
(159) Whittaker, E. T. *Proc. R. Soc. Edinburgh* **1915**, *35*, 181.
(160) Nyquist, H. *Trans. AIEE* **1928**, *47*, 617.
(161) Shannon, C. E. *Proc. IRE* **1949**, *37*, 10.

TABLE I: Isotropic Sampling Efficiency[a]

dim.	η_{max},[b] %	η_{cub},[c] %	η_{max}/η_{cub}[d]
1	100.0	100.0	1.0
2	90.7	78.5	1.15
3	74.0	52.4	1.4
4	61.7	30.8	2.0
5	46.5	16.45	2.8
6	37.3	8.07	4.6
7	29.5	3.69	8.0
8	8.07	0.505	16.0

[a] Data from ref 162. [b] Maximum sampling efficiency. [c] Efficiency of cubic lattice. [d] Improvement factor.

is determined by (2.12). This implies that a value of a point between sampling points can be interpolated with any desired accuracy. This theorem also implies a faithful representation of the nth derivative of the function inside the supported interval.

The most simple generalization of the Fourier method to multidimensions is the use of an equally spaced Cartesian grid. An important observation is that this grid is not isotropic in momentum space, so that different directions have different sampling intervals. Although a completely isotropic grid is not possible, the sampling positions can be optimized to construct the optimum isotropic grid in momentum space. It has been shown[113,162] that the optimal sampling points are equivalent to the centers of multidimensional densely packed hard spheres.[163] The free volume between the spheres is wasted phase volume. As a result, in multidimensions, the limit of one sampling point per unit volume is not obtainable even for optimal packing. Table I compares the sampling efficiency of a cubic grid with the optimal grid as a function of dimension. One can notice that the importance of optimal sampling is enhanced with dimensionality. Nevertheless, even the optimal sampling efficiency decreases with dimensionality; for example, for six dimensions 2.7 sampling points are needed per unit volume, compared to 12.4 points in the Cartesian cubic lattice.

As has been shown, a confined function in phase space can be represented with no loss of accuracy. In realistic problems, the wave function cannot be confined, which means that it is not strictly band limited with finite support. The idea of a wave packet which is a wave function that is almost band limited is central to the use of the discrete representation. A wave packet is a wave function that is semilocalized in phase space. The most well-known example is the Gaussian wave packet. Although the wave function is not confined to a finite volume, the amplitude out of this volume in phase space converges exponentially to zero when the volume is increased. This exponential convergence is typical of a good representation of phase space.[164] A counter example is supplied by a rectangular packet which has been reported in the literature.[86] In coordinate space the wave function is well confined, but in momentum space the rectangular wave function is transformed to $\psi(k) = [\sin(a(k-k_0))/[a(k-k_0)]$, which has only a linear convergence rate with the size of the grid in $\boldsymbol{k}$ space.

II.4. Representation of Operators. The construction of the discrete Hilbert space enables the representation of operators. The collocation method allows the calculation of local as well as nonlocal operators as was demonstrated by (2.5). A more appealing quantum-mechanical description is to calculate the operation of operators through their discrete spectrum. The most important operator is the Hamiltonian operator. The result of its operation $\phi = \hat{H}\psi$ is the key to the time evolution step. The Hamiltonian operator is partitioned in the usual fashion between kinetic and potential operators $\hat{H} = \hat{T} + \hat{V}$. The strategy is to calculate each operator locally. The potential operator is already local in coordinate space, and therefore its operation is simply a multiplication of $V(x_j)$ by $\psi(x_j)$. A local operation of the kinetic energy operator is possible in momentum space where it becomes a multiplication by the kinetic energy discrete spectrum:

$$T(k) = \hbar^2 k^2/2m \tag{2.14}$$

To summarize, the kinetic energy operator is calculated by transforming ψ to momentum space by a forward FFT, multiplying by $T(k)$, and performing an inverse FFT back to coordinate space.[94] It has been shown[94] that this spectral representation preserves the coordinate momentum commutation relations which are the heart of quantum mechanics. An important issue in representing the kinetic energy operator is that it must be Hermitian. Otherwise instabilities arise in the propagation.

The Fourier spectrum can be compared to the spectrum of the finite difference (FD) method[165] by noticing that the finite difference operator, $\hat{T}_{FD}f_j = -\hbar^2(f_{j+1} + f_{j-1} - 2f_j)/2m\Delta x^2$, is a member of the family of convolution operators and therefore is diagonal in $\boldsymbol{k}$ space. Performing a Fourier transform, the spectrum in $\boldsymbol{k}$ space of the FD kinetic energy operator is obtained:

$$\hat{T}_{FD}(k) = -\frac{\hbar^2}{2m}\frac{2(\cos(k\Delta x) - 1)}{\Delta x^2} = \frac{\hbar^2}{2m}\left[\frac{2\sin(k\Delta x/2)}{\Delta x}\right]^2 \tag{2.15}$$

Upon comparing the spectra, it is apparent that, as k increases, the finite difference spectrum deviates more and more from the correct value. It is usually assumed that acceptable accuracy in the FD method is obtained when at least 10 points are used per wave period, which means also 10 points per unit volume in phase space. The finite difference algorithms are based on a local polynomial approximation of the wave function; therefore the convergence of the method follows a power law of $(\Delta x)^n$, where n is the order of the finite difference approximation. The local description leads to a poor spectral representation of the kinetic energy operator. As a result of this semilocal representation of the momentum operator, the commutation relations of quantum mechanics are not strictly obeyed. The finite difference methods scale linearly with the phase-space volume because they cannot account for all the nonlocal character of quantum mechanics.

In a rectangular set of multidimensional coordinates, the kinetic energy operator is separable

$$\hat{T} = \frac{\hbar^2}{2m}\sum_{i=1}^{D}\boldsymbol{K}_i^2 \tag{2.16}$$

where $\boldsymbol{K}_i$ is the vector of k values in spatial dimension i. For the optimal packing case[113] or other skewed sets of coordinates, the kinetic energy operator becomes

$$\frac{\hat{P}^2}{2m} = \frac{\hbar^2}{2m}\boldsymbol{K}\cdot\tilde{\mathbf{G}}\cdot\boldsymbol{K} \tag{2.17}$$

where $\boldsymbol{K}$ is the vector of k values for each spatial direction and $\tilde{\mathbf{G}}$ is a positive definite matrix connecting spatial direction i with direction j. Reference 113 describes the Fourier implementation for the skewed multidimensional coordinate system.

The idea of a space in which a local representation of the operator is possible can be carried beyond Cartesian coordinates and the kinetic energy operator. A local representation is the most efficient way to implement a numerical scheme. Work on these lines has been carried out for the representation of the kinetic energy operator in spherical coordinates:[100,127]

$$\frac{\hat{P}^2}{2m} = -\frac{\hbar^2}{2m}\left[\frac{1}{r^2}\frac{\partial}{\partial r}r^2\frac{\partial}{\partial r} + \frac{1}{r^2\sin\theta}\frac{\partial}{\partial\theta}\sin\theta\frac{\partial}{\partial\theta} + \frac{1}{r^2\sin^2\theta}\frac{\partial^2}{\partial\theta^2}\right] \tag{2.18}$$

The representation problem can be divided into radial and angular parts. For the radial part of the Laplacian, the Bessel function $J_{1/2}(r)$ is an eigenvalue. This means that, by using a Bessel transform, the radial part of the Laplacian becomes a local op-

(162) Petersen D. P.; Middelton, D. *Inf. Contr.* **1962**, *5*, 279.
(163) Rogers, C. A. *Packing and Covering*; Cambridge University Press: Cambridge, 1964.
(164) Tadmor, E. *SIAM J. Numer. Anal.* **1986**, *23*, 1.
(165) Miller, K. S. *An Introduction to Calculus of Finite Difference and Difference Equations*; Henry Holt and Co.: New York, 1960.

erator with the spectrum $-k^2$. Moreover, using the transform with $J_{l+1/2}$, one can include the centrifugal part of the Laplacian, $l(l+1)/r^2$, when a Y_{lm} expansion is used in the operator eliminating the singularity at the origin. Technically fast Bessel transforms have been reported in the literature which scale as $O(N \log N)$ with the number of grid points N.[166] A local description of the angular part has not yet been reported. For the ϕ coordinate, the Fourier method is applicable. For θ, a discrete variable representation with Legendre quadrature points has been suggested.[167] Care must be taken that the ϕ grid points are staggered for each θ layer. For an angular momentum l, there will be l^2 sampling points. Because a fast Legendre transform is not known, the method will scale as $Q(l^3 \log l)$. For small values of l, direct expansion in Y_{lm}[122-128] functions is more efficient than the spectral method. The scaling becomes $O(l^4)$. Other collocation methods can have advantages in cases where boundary conditions have to be matched or to include singular operators such as the Coulomb potential $V(r) = -(e^2/r)$.[168]

II.5. Flexibility. One of the most important qualities of the representation strategy described here is its flexibility. This is because different degrees of freedom can be treated by different methods, and the total representation can be combined to give a vector representation of $\phi = \hat{H}\psi$. As was mentioned in the previous section, a partial expansion is one of the most useful options that has been applied to rotational states.[122-128] A straightforward application of this idea is in the treatment of nonadiabatic phenomena as motion on more than one potential energy surface.[110,145]

One of the methods to minimize the computational effort is to use an adoptive grid, a grid which changes as the calculation progresses. For example, in a reactive scattering calculation for the initial state representation, it is enough to include only the entrance channel and then, when the wave packet evolves to enlarge the grid, to include also the reactive channel. The key element in this program is an interpolation scheme that allows grid-to-grid transfer of the wave function. The collocation method, besides allowing the representation of nonlocal operators, is also an extremely accurate and efficient interpolation scheme.[169] In the same spirit, the work of Heather and Metiu[135] has demonstrated the use of the superposition principle to split the propagation onto two overlapping grids. This method allows the separation of the asymptotic dynamics from the interaction part. Care must be taken that the transmission of amplitude from one grid to the other is gradual in space to avoid numerical problems of overflowing phase space by a sharp transmission function.

The possibility of optimizing the representation method and adopting it to the current extent of the wave function allows a very flexible computational scheme.

II.6. Initial Wave Packet. The choice of the initial wave packet depends on the purpose of the calculation. For the translational asymptotic degree of freedom, a Gaussian wave packet is the common choice because it allows good control of its extent in phase space. The choice of the width of the Gaussian wave packet depends on the purpose of the calculation. For example, in the simulation of a gas–surface collision, the width of the packet can be chosen to match the energy spread of the experimental supersonic beam. Other applications, such as the determination of $\hat{S}$ matrix elements, are optimal with a wide energy range. This means a narrow wave packet in position. For bound asymptotic degrees of freedom, it is customary to chose an eigenstate as the initial condition (see section III.5). The total initial wave packet is constructed as a product of the wave packets of different degrees of freedom, for example, $\psi(x,y,z) = \phi(x)\xi(y)\chi(z)$.

II.7. Computational Considerations. The collocation method that has been described in this section has many advantages. First, flexibility allows the efficient modeling of a large variety of systems. The computational scaling varies from $O(N)$ to $O(N^2)$. Moreover, the algorithms developed from the collocation methods are highly vectorizable, an important consideration since modern computers gain their speed from parallel and vector type architecture. In particular, the FET algorithm has extremely efficient implementation.[150] The representation procedure for the Hamiltonian operator, as will be described in the next section, is used recursively. It is found that if the representation is not completely Hermitian, the propagation scheme can become unstable.

III. Time Propagation

III.1. Once the solution to representing the wave function and the Hamiltonian operation has been found, the problem of propagating the wave function has to be addressed. Formally the time-dependent Schrödinger equation has the solution

$$\psi(t) = \hat{U}(t)\psi(0) = \hat{T}\exp\left[-\frac{i}{\hbar}\int_0^t \hat{H}\,dt'\right]\psi(0) \quad (3.1)$$

where $\hat{T}$ is the time-ordering operator. An approximation of this equation presents the following difficulties: first, exponentiation of the Hamiltonian operator and, second, the construction of the time-ordering operator, $\hat{T}$.

Before reviewing the existing solutions for these difficulties, one can consider the limitations imposed on the propagation by the time–energy uncertainty principle. These limitations are common to all propagation schemes and therefore serve as a common denominator for comparison. In analogy to the momentum coordinate phase space, the time–energy phase space can be considered. The volume of this phase space in units of $\hbar$ determines the minimum number of points needed to propagate the system in time intervals Δt with energy range ΔE.

For each discrete representation, one can estimate the range of eigenvalues of the Hamiltonian operator $\Delta E = E_{max} - E_{min}$. For example, in the Fourier representation the range can be estimated by adding the upper and lower bounds of the kinetic and potential energy represented on the grid:

$$E_{max} = V_{max} + K_{max} \quad (3.2)$$

where

$$K_{max} = \sum_i \frac{\pi^2\hbar^2}{2m_i(\Delta q_i)^2} \quad (3.3)$$

where m_i and Δq_i are the mass and grid spacing of the ith coordinate and

$$E_{min} = V_{min} \quad (3.4)$$

Once ΔE is known, the time–energy phase space with volume $\Delta E t$ can be considered. This volume gives a lower bound to the number of steps in the time propagation. This also can be understood by noticing that a time step cannot be larger than the smallest period determined by $\hbar/E_{max}$.

If the Hamiltonian in (3.1) is time independent, the time-ordering operator, $\hat{T}$, can be omitted, resulting in great simplification. The strategy for solving time-dependent problems is to divide the total evolution operator into short segments in which the Hamiltonian does not change significantly:

$$\hat{U}(t) = \prod_{n=0}^{N-1} \hat{U}((n+1)\Delta t, n\Delta t) \quad (3.5)$$

where $\Delta t = t/N$. It will be shown that global propagators which use a polynomial expansion of $\hat{U}(t)$ are more accurate and efficient than short-time propagators. Nevertheless, for time-dependent problems one can only use short-time approximation.

III.2. Global Propagators: The Chebychev and Laczos Schemes. The main idea in a global propagator is to use a polynomial expansion of the evolution operator:

$$\hat{U}(t) = e^{(-i/\hbar)\hat{H}t} \approx \sum_{n=0}^{N} a_n P_n\left(-\frac{i}{\hbar}\hat{H}t\right) \quad (3.6)$$

The problem then becomes the choice of the optimal polynomial approximation.

(166) Talman, J. D. *J. Comput. Phys.* **1978**, *29*, 35. *J. Comput. Phys.* **1978**, *30*, 93.
(167) Light, J. C., private communication.
(168) LeForestier, C.; Kosloff, R., work in progress.
(169) Bisseling, R. H.; Kosloff, R.; Kosloff, D. *Comput. Phys. Commun.* **1986**, *39*, 313.

The Chebychev scheme[99] approaches this problem in analogy to the approximation of a scalar function. Consider a scalar function $F(x)$ in the interval $[-1, 1]$. In this case it is known that the Chebychev polynomial approximations are optimal since the maximum error in the approximation is minimal compared to almost all possible polynomial approximations.[170]

In the approximation of the evolution operator, the complex Chebychev polynomials $\Phi_n(\hat{X})$ are used, replacing the scalar function by a function of an operator. In making this change, one has to examine the domain of the operator and adjust it to the range of definition of the Chebychev polynomials. The range of the definition of these polynomials is from $-i$ to i. This means that the Hamiltonian operator has to be renormalized by dividing by $\Delta E = E_{max} - E_{min}$. Also, for maximum efficiency, the range of eigenvalues are positioned from -1 to 1 by shifting the Hamiltonian to

$$\hat{H}_{norm} = 2\frac{\hat{H} - \hat{I}(\frac{1}{2}\Delta E + V_{min})}{\Delta E} \tag{3.7}$$

With this definition, the evolution of the wave function ψ can be approximated as

$$\psi(t) \approx e^{(-i/\hbar)((1/2)\Delta E + V_{min})t} \sum_{n=0}^{N} a_n\left[\frac{\Delta E t}{2\hbar}\right]\Phi_n[-i\hat{H}_{norm}]\psi(0) \tag{3.8}$$

where Φ_n are the complex Chebychev polynomials. The first term in the right-hand side is a phase shift compensating the shift in the energy scale. The expansion coefficients become

$$a_n(\alpha) = \int_{-i}^{i} \frac{e^{i\alpha x}\Phi_n(x)\,dx}{(1-x^2)^{1/2}} = 2J_n(\alpha) \tag{3.9}$$

and $a_0(\alpha) = J_0(\alpha)$ and $\alpha = \Delta E t/\hbar$. Considering the propagation algorithm, the use of (3.8) requires the calculation of the operation of $\Phi_n(-i\hat{H}_{norm})$ on $\psi(0)$. This is calculated by using the recursion relation of the Chebychev polynomials

$$\phi_{n+1} = -2i\hat{H}_{norm}\phi_n + \phi_{n-1} \tag{3.10}$$

where $\phi_n = \Phi_n(-i\hat{H}_{norm})\psi(0)$. In order to save storage, only the vectors that are the result of the n and $n-1$ operation are saved. The result is accumulated in ψ. The number of expansion terms needed to converge the sum in (3.8) is determined by the size of the time–energy phase-space volume: $\alpha = \Delta E t/\hbar$. Examining the expansion coefficients as a function of n, one finds that when n becomes larger than α, the Bessel functions $J_n(\alpha)$ decay exponentially. This means that, in a practical implementation, the maximum order N can be chosen such that the accuracy is dominated by the accuracy of the computer. The total number of expansion terms will be slightly larger than the theoretical limit $\Delta E t/\hbar$. One of the most important aspects of the Chebychev propagation scheme is that the error is uniformly distributed over all the range of eigenvalues. Numerical examples have shown that a practical algorithm can be constructed confirming all the mathematical predictions.[99]

One drawback of a global evolution method is that intermediate results, which may carry much information, are not obtained. One way to overcome this problem is to split the propagation into smaller intervals. The practical lower limit of the Chebychev expansion is 40 terms. The reason is that the extra terms above $n = \alpha$ which are needed to converge the sum begin to dominate, making the approximation inefficient. For interpretation of intermediate results, this time interval is usually enough, but many applications require the calculation of correlation functions at very short intervals. The problem can be overcome by considering that only the expansion coefficients in (3.8) are time dependent. The Chebychev polynomial operations, $\phi_n = \Phi_n(-i\hat{H}_{norm})\psi(0)$, which require most of the calculation effort, are time independent. This means that the expansion coefficients a_n can be recalculated for many intermediate times. For example, when the correlation function $\langle\xi(0)|\hat{O}|\psi(t')\rangle$ is desired at an intermediate time t', it can be approximated by

$$\langle\xi(0)|\hat{O}|\psi(t')\rangle \approx \sum_{n=0}^{N} a_n\left(\frac{\Delta E t'}{\hbar}\right)\langle\xi(0)|\hat{O}|\phi_n\rangle \tag{3.11}$$

Notice that the accumulator which is the right-hand side of (3.11) is scalar and therefore the storage requirements of the calculation are only slightly increased.

One of the most important correlation functions in molecular dynamics is when $\hat{O} = \hat{\mu}$, the dipole operator. It has been shown that the absorption,[171,172] Raman,[171,173] and CARS spectra[174] can be calculated by using Fourier transforms of these correlation functions. For example, the Raman spectrum becomes

$$\alpha_{fi}(\Delta\omega) \approx \frac{i}{\hbar}\int_0^\infty e^{-i\omega t}\langle\psi_i(0)|\hat{\mu}|\psi_f(t)\rangle\,dt \tag{3.12}$$

where $\alpha_{fi}(\Delta\omega)$ is the Raman amplitude from an initial state i to a final state f with frequency difference $\Delta\omega$ and where the evolution of the state i is on the upper electronic surface. Applying this formula with (3.11) and changing the order of the sum and integral, one finds that the spectrum becomes

$$\alpha_{fi}(\Delta\omega) = \frac{i}{\hbar}\sum_{n=0}^{N} b_n(\Delta\omega)\langle\psi_i(0)|\hat{\mu}|\phi_n\rangle \tag{3.13}$$

where $\hat{H}_{norm}$ is the upper state normalized Hamiltonian, and the new expansion coefficients b_n are the half Fourier transforms of the Bessel functions $a_n(\Delta E t/\hbar)$:

$$b_n(\Delta\omega) = \frac{2i}{(\Delta E^2 - \Delta\omega^2)^{1/2}}\left[\sin\left[n\arcsin\left(\frac{\Delta\omega}{\Delta E}\right)\right] + i\cos\left[n\arcsin\left(\frac{\Delta\omega}{\Delta E}\right)\right]\right] \tag{3.14}$$

and

$$b_0 = i/[(\Delta E^2 - \Delta\omega^2)^{1/2}]$$

Similar formulas can be obtained for the absorption and CARS spectra. Figure 2 displays the Raman spectra of a photodissociating molecule. The Morse potential is used for the ground state.

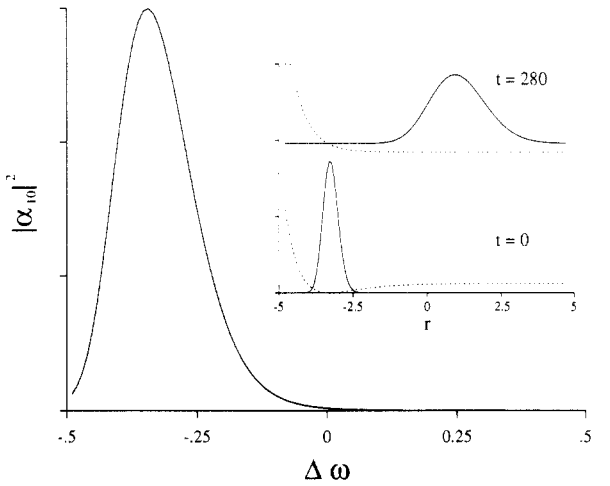

Figure 2. Raman spectrum of ground-state Morse oscillator and an excited-state repulsive potential. The lower panel shows the spectra $|\alpha_{10}|^2$ as a function of $\Delta\omega$. The broad line is a result of the fast photodissociation on the upper repulsive potential. The upper right panel shows the ground-state initial state and the ground-state potential (dashed line) and the upper state wave function after 280 au of time on the repulsive potential (dashed line). The Morse potential parameters are $D_0 = 0.174$ au, $\beta_0 = 0.9374$ au^{-1}, and mass $m = 911$ au. The upper repulsive potential parameters are $D_1 = 0.164$ au and $\beta_1 = 0.9374$ au^{-1}. A grid of 128 points was used with $\Delta x = 0.075$ au. The number of Chebychev coefficients in the calculation was 436.

(170) Smirnov, V. I.; Lebedov, M. A. *Functions of a Complex Variable*; ILIFFE Books: London, 1968.

(171) Hizhanykov, V. V.; Tehver, I. J. *Opt. Commun.* **1977**, *22*, 49.
(172) Heller, E. J. *J. Chem. Phys.* **1976**, *65*, 63.
(173) Tannor, D. J.; Heller, E. J. *J. Chem. Phys.* **1982**, *77*, 202.
(174) Tannor, D. J.; Rice, S. A.; Weber, P. M. *J. Chem. Phys.* **1985**, *83*, 6158.

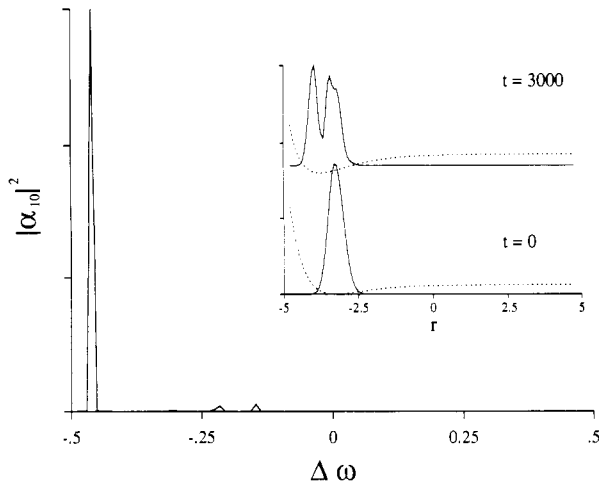

Figure 3. Raman spectrum of ground-state Morse oscillator and an upper modified Morse potential. The lower panel shows the Raman spectra. Sharp features can be seen due to the bound upper surface. The upper right panel shows the initial state and the upper state after 3000 au of time. The upper state is clearly bound. The upper potential has the form $V(r) = D_1[\exp(-2\beta_1 r) - c_1 \exp(-\beta_1 r)]$, where $D_1 = 0.164$ au, $\beta_1 = 0.9374$ au^{-1}, $c_1 = 1.5$, and r_0 was shifted from the ground state by 0.1 au. The number of Chebychev coefficients in the calculation was 4596. Even with this very large Chebychev expansion the norm and energy were conserved to the accuracy of the computer, demonstrating the stability of the Chebychev recursion.

A repulsive exponential potential is used for the excited state. Converged results were obtained for a relatively short propagation because the wave function moves away from the excitation zone. Figure 3 displays the Raman spectra of a system with a bound excited state. The period of propagation was approximately 10 times longer than that in Figure 2. Notice the stability of the Chebychev recurrence, which was carried out to order 4596. The overhead involved in the calculation is minor compared to the propagation of the wave function. In calculating the spectra for more complicated systems, this method is most efficient when the propagation on the excited surface is short. The coefficients b_n converge very slowly with n; therefore the convergence of the expansion must come from the motion of the wave function on the excited surface. Such a situation is found in photodissociation experiments for which the method will find many applications.

Recently in molecular dynamics the use of the Lanczos recurrence expansion[175,176] has been used for time propagation. Writing the Lanczos recurrence relation

$$\beta_j \phi_{j+1} = [\hat{H} - \alpha_j]\phi_j - \beta_{j-1}\phi_{j-1} \tag{3.15}$$

where

$$\alpha_j = \langle \phi_j | \hat{H} | \phi_j \rangle$$

β_j is obtained by the normalization requirement:

$$\langle \phi_{j+1} | \phi_{j+1} \rangle = 1$$

and $\beta_0 = 0$. For propagating in time, the recurrence is started in the same way as the Chebychev method $\phi_1 = \psi(0)$. The outcome of the recurrence is a set of orthogonal vectors in which the Hamiltonian matrix becomes tridiagonal. Remembering that the Chebychev and the Lanczos recurrence are both independent of the representation and that they have been applied to similar problems, it is desirable to compare the methods. So far this has not been attempted.

Park and Light[144] estimate that the error in the Lanczos expansion for a time-dependent propagation behaves as in a Taylor expansion. The convergence properties of the Taylor expansion behave as a power law, which is a slower convergence than the exponential law of the Chebychev expansion. Moreover, unlike the Chebychev method for which the error is distributed uniformly for all eigenvalues, the error in the Lanczos method is larger for larger eigenvalues. On the other hand, the Lanczos vectors ϕ are orthogonal and can be used as a base to diagonalize the Hamiltonian matrix which is tridiagonal in this representation. The Chebychev vectors ϕ are not orthogonal. Another advantage of the Lanczos method is that one does not have to normalize the Hamiltonian. Nevertheless, the Lanczos recursion is not stable and therefore requires stabilization techniques, unlike the Chebychev method for which the recursion is stable. Runs using more than 4000 terms have been used (see Figure 3). The most important point is that in most applications the Chebychev and Lanczos recurrence schemes are interchangeable.

III.3. Short-Time Propagators. In many physical situations, time-dependent Hamiltonian operators are used. Examples include motion in high laser fields, motion under thermal agitation, or the TDSCF approximation. In this case it is appropriate to use a short-time propagation scheme.

The Second-Order-Differencing Scheme (SOD). The simplest scheme for prpagating (1.1) is to expand the evolution operator $\hat{U} = \exp(-i\hat{H}\,dt/\hbar)$ in a Taylor series:

$$\exp(-i\hat{H}\,dt/\hbar) = 1 - i\hat{H}\,dt/\hbar + \ldots \tag{3.16}$$

It has been found that a numerical scheme based on this expansion is not stable.[85] The instability comes about because the scheme does not conserve the time reversal symmetry of the Schrödinger equation. With a symmetric modification of the expansion, stability is obtained. One way to formulate the scheme is to use second-order differencing (SOD) to approximate the time derivative in (1.1). Another formulation uses the symmetric relation

$$\psi(t+dt) - \psi(t-dt) = (e^{-i\hat{H}dt/\hbar} - e^{i\hat{H}dt/\hbar})\psi(t) \tag{3.17}$$

and then by expanding $\hat{U} = \exp(-i\hat{H}\,dt/\hbar)$ and $\hat{U}^*$ in a Taylor series, the explicit second-order propagation scheme is obtained:

$$\psi(t+\Delta t) \approx \psi(t-\Delta t) - 2i\Delta t\hat{H}\psi(t)/\hbar \tag{3.18}$$

This is the time propagation scheme used in the finite difference method of Askar and Cakmak[85] and also in the Fourier method.[94,95,101]

If the Hamiltonian operation is Hermitian, which is the case for both the FD method and the Fourier method, the SOD propagation scheme preserves norm and energy. A good way to investigate this is to write the propagation as a discrete mapping scheme:

$$\begin{bmatrix} \psi^{n+1} \\ \psi^{n} \end{bmatrix} = \begin{bmatrix} 1 - 4\Delta t^2\hat{H}^2/\hbar^2 & -2i\Delta t\hat{H}/\hbar \\ -2i\Delta t\hat{H}/\hbar & 1 \end{bmatrix} \begin{bmatrix} \psi^{n-1} \\ \psi^{n-2} \end{bmatrix} \tag{3.19}$$

where n is the index of the time step. The eigenvalues of this propagation matrix are

$$\lambda_{1,2} = 1 - 2\Delta t^2\hat{H}^2/\hbar^2 \pm \frac{2\Delta t\hat{H}}{\hbar}\left[\frac{\Delta t^2\hat{H}^2}{\hbar^2} - 1\right]^{1/2} \tag{3.20}$$

The discrete map is area preserving if the determinate of the propagation matrix is unity which is equivalent to $\lambda_1\lambda_2 = 1$. This implies the norm conservation[94]

$$\langle \psi^{n+1} | \psi^{n} \rangle = \text{const} \tag{3.21}$$

The discrete map is stable only if the eigenvalues $\lambda_{1,2}$ are complex. Real eigenvalues lead to exponential growth as λ_1^n because $\lambda_1 > 1$. This leads to the stability criterion of the discrete map:

$$\Delta t^2\hat{H}^2/\hbar^2 - 1 < 0 \tag{3.22}$$

which has to be true for all eigenfunctions of the Hamiltonian operator leading to

$$\Delta t \leq \hbar/E_{\max} \tag{3.23}$$

where $E_{\max}$ is the largest (positive or negative) eigenvalue of the discrete Hamiltonian. If the time step exceeds the stability limit, exponential solutions take over, resulting in a numerical overflow. This fact can be used to obtain empirically the stability limit.[94]

(175) Nauts, A.; Wayatt, R. E. *Phys. Rev. Lett.* **1983**, *51*, 2238.
(176) Lanczos, C. *J. Res. Natl. Bur. Stand.* **1950**, *45*, 255.

The norm and energy conservation of the SOD scheme is a consequence of the time reversal symmetry of the scheme and of the Hermitian property of the Hamiltonian operator for both the FD and Fourier methods. The energy conservation is obtained in a similar way by multiplying (1.1) by $\partial\psi^{*n}/\partial t$. The result is

$$\mathrm{Re}\ \langle\psi^{n+1}|\hat{H}|\psi^{n}\rangle = \mathrm{const} \tag{3.24}$$

Because of this norm and energy conservation, the error in propagation accumulates in the phase. In order to obtain an estimate of this error, consider the propagation of an eigenfunction ϕ_m with eigenvalue $\mathbf{E}_m$. The eigenvalues of the propagation matrix become

$$\lambda_{1,2} = 1 - \frac{2\Delta t^2\mathbf{E}_m^2}{\hbar^2} \pm \frac{2\Delta t\mathbf{E}_m}{\hbar}\left[\frac{\Delta t^2\mathbf{E}_m^2}{\hbar^2} - 1\right]^{1/2} \tag{3.25}$$

By comparing (3.24) with the eigenvalues of the exact propagation operator, $\lambda_{12} = e^{\pm 2i\mathbf{E}_m\Delta t/\hbar}$, one finds that the error in propagation by the SOD method per time step is

$$\text{error} \approx \frac{(\Delta t\mathbf{E}_m)^3}{3\hbar^3} \tag{3.26}$$

Propagating N times, this error accumulates N times. First, it should be noticed that the error is not uniform and is large for large eigenvalues of ψ. To minimize the error in phase, it is customary to choose a time step, Δt, 5 times smaller than the stability limit, $\Delta t < \hbar/5E_{\max}$. The resulting error for N steps becomes: error $\approx N/375$, which allows a few hundred propagation steps before errors in interference terms become important. For calculations pertaining to a thermal surface, phase coherence is important only for relatively short periods of time. Therefore, the SOD scheme is a good choice for these problems. One should notice that, by shifting the energy and by adding a constant to the Hamiltonian, one can predetermine the region in energy with minimum error.

The Split Time Propagation Scheme. Feit and Fleck[117-119] have introduced a split time propagation scheme in which the kinetic operator and potential operator are used to propagate the wave function separately:

$$\exp(-i\hat{H}\Delta t/\hbar) \approx \exp\left(-i\frac{\hat{P}^2}{2m}\frac{\Delta t}{2\hbar}\right)\exp\left(-i\hat{V}\frac{\Delta t}{2\hbar}\right)\times \exp\left(-i\hat{V}\frac{\Delta t}{2\hbar}\right)\exp\left(-i\frac{\hat{P}^2}{2m}\frac{\Delta t}{2\hbar}\right) \tag{3.27}$$

Each of these propagations is carried out in a local representation: first, the wave is transformed to $\boldsymbol{k}$ space by an FFT procedure and then multiplied at each grid point by $\exp(-i(\hat{P}^2/2m)(\Delta t/2\hbar))$; afterward the wave function is transformed back to coordinate space by an inverse FFT procedure, and finally the wave function is multiplied by $\exp(-i\hat{V}(\Delta t/2\hbar))$, and $^1/_2$ time step of propagation is complete. The next half step is done in reverse order with the potential energy propagation made before the kinetic energy propagation. The split operator method can be used when a transformation is found from a diagonal kinetic energy representation to a diagonal potential energy representation. The method has been used only in relation to the Fourier representation.

Norm is strictly conserved by the split time scheme, because each split time step is unitary. Error is due to the noncommutability of the kinetic and potential operators. Because of the alternating propagation scheme, the first term in the expansion $\Delta t^2[\hat{P}^2,\hat{V}]/(8m\hbar^2)$ cancels out; therefore, errors are of $O(\Delta t^3)$ (see also ref 141).

$$\text{error} \approx \max\left[-i\frac{\Delta t^3}{16m}[\hat{V},[\hat{V},\hat{P}^2]],\ -i\frac{\Delta t^3}{32m^2}[\hat{P}^2,[\hat{P}^2,[\hat{V}]]]\right]/\hbar^3 \tag{3.28}$$

This error accumulates in both the phase and energy of the wave function. The usual method of estimating the error by propagating an eigenvalue of the Hamiltonian is not usable. For the specific case of an harmonic oscillator the error can be estimated by considering propagation of a Gaussian wave packet since this fundamental form is invariant to the split operator propagation. It is found that the error is linear in the quantum number n. A method to check the error empirically is to follow the energy deviation from the initial value because the method does not conserve energy. For multichannel problems the split operator method becomes cumbersome because of the need to diagonalize the potential energy at each grid point.

Other existing and implicit propagation schemes based on a Taylor expansion of the evolution operator $\hat{U}$ can be found, such as the Crank–Nicholson method[84] or an implicit split method.[91]

Two time scales appear in the short-time propagators. The first is the stability time limit and the second is the convergence limit. The stability limit is determined by the time–energy uncertainty limit $\Delta t_s = \hbar/E_{\max}$. In the SOD scheme a time step larger than Δt_s will cause exponential divergence. The split operator method is intrinstically stable. Nevertheless, a time step larger than Δt_s is meaningless because then the phase of the propagation operator exceeds 2π. The convergence time step Δt_c is determined by the desired accuracy. All short-time propagation methods accumulate errors. Considering a situation where an upper bound is imposed on the error for a long-time propagation, the time step Δt_c has to be reduced to compensate for the accumulated error for longer propagation times. Both the SOD method and the split operator method are second order in time, which means that the time step is reduced by a factor of $t^{1/2}$. The result is that the numerical effort will scale as $O(t^{3/2})$ for both methods. Using a higher order method becomes advantageous for longer times because in general the computation of a method of order m will scale as $O(t^{1+1/m})$. In both methods the error is not uniformly distributed. In the SOD method the error can be minimized by shifting the potential by a constant. In the split operator method the largest error is expected where the potential has the largest variation. The time step Δt_c is then chosen so that the error becomes acceptable. It should be emphasized that Δt_c has to be smaller than Δt_s. If for a particular choice of grid parameters Δt_c is larger than Δt_s, this means that computation savings can be obtained by trimming the grid.

III.4. Interpretation. One of the most attractive aspects of time-dependent methods is that much insight can be obtained by inspecting snapshots of the wave function at regular time intervals. Such an inspection can lead to an identification of mechanisms in analogy to the insights obtained from classical trajectories. The use of graphic tools for quantum-mechanical calculations needs some adjustment, however, because of the global description of the wave function. Typically, one inspects the square amplitude of the wave function in coordinate or in momentum space. Figure 4 shows the details of mechanism of the reaction F + DBr → FD + Br. Figure 5 shows a surface scattering event in momentum space. The diffraction peaks which are the result of the collision can be identified clearly. Other useful representations include flux maps[84] and phase maps.

A more rigorous approach in analysis relies on the fact that, in the asymptotic part of the grid, the energy transfer between the different degrees of freedom halts. The system is then divided into bound and free degrees of freedom. At this point the overlap with the asymptotic bound degrees of freedom is calculated, from which transition probabilities can be obtained. In the case of a time-independent Hamiltonian, one column of the $\tilde{\mathbf{S}}$ matrix can be extracted for a range of energies. This is done by observing that because of the conservation of energy, the unbound degree of freedom can be analyzed, associating each final-state momentum component uniquely with an initial momentum component.[122]

In many scattering events there is a time-scale separation between a direct scattering event and a delayed part which may be a resonance. In problems where one is interested in studying the decay of the resonance, grid space can be saved by using absorbing boundary conditions, based on a slowly varying optical potential.[177]

(177) Kosloff, R.; Kosloff, D. *J. Comput. Phys.* **1986**, *63*, 363.

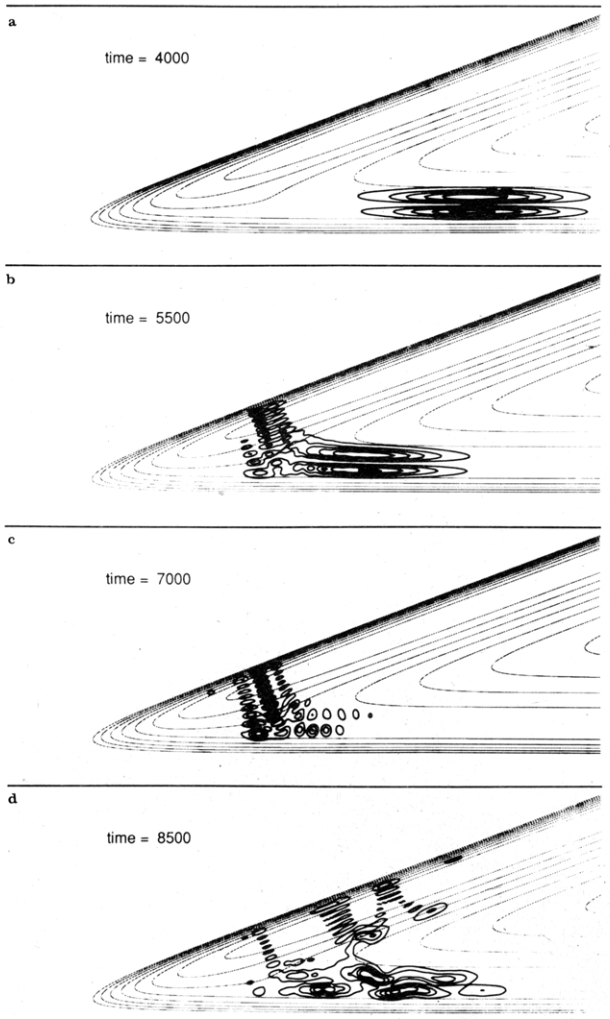

Figure 4. Snapshots of the squared amplitude of the wave function for the reactive system F + DBr → FD + Br. Panel a shows the system in the reactant channel. The initial vibration is $v = 1$, and a Gaussian wave function is used for the initial translation. Panel b shows the wave function entering the interaction zone. The deuterium is vibrating violently between the fluorine and bromine atoms. Part of the wave function is starting to be reflected from the downhill slope of the potential (a pure quantum effect). Panel c shows a more developed wave function in the reactive zone. A breathing mode of the fluorine/bromine mode is identified while the deuterium is continuing to vibrate. The reflected wave function is interfering with the incoming wave function in the entrance channel. In panel d the wave function splits into the reactive and nonreactive channels. Part of the wave function is seen cutting the corner. The initial energy is $E = 0.122\,643$ hartree, enough to populate $v = 7$ in the reactive channel. The Fourier Chebychev method was used for the propagation. (Adopted from A. D. Hammerich, R. Kosloff, and M. A. Ratner, unpublished results.)

III.5. Sidetrack: Calculation of Eigenfunctions. An offshoot of time-dependent quantum-mechanical methods is the calculation of eigenfunctions and eigenvalues without a full diagonalization of the Hamiltonian matrix. These eigenfunctions are usually used for constructing the initial wave function or for asymptotic analysis. One such method is to use a propagation in imaginary time to obtain the ground state. This propagation is made by using the Chebychev scheme resulting in exponential convergence.[106] Higher eigenstates are obtained by filtering out the ground state and other lower energy states and resuming the relaxation. This method is optimal when only a small set of lower eigenfunctions is needed out of a very large problem.

A very useful method for obtaining eigenvalues is by examining the Fourier transform of the autocorrelation function, a use originated by Feit and Fleck.[117] An implementation of this idea can be made by using the Chebychev propagation method employing formulas similar to the ones used to obtain the spectra. The method is particularly fit for obtaining eigenvalues under the TDSCF approximation[146] (see next section).

Another method applicable for highly excited eigenstates is to start from a known simple separable system for which the eigenfunctions are known and then adiabatically switching the interaction. This method has been tested by using the SOD time propagation scheme, giving good results.[178]

The advantage of these methods is that, because they are aimed at obtaining only a few eigenvalues, they scale as $O(N \log N)$ compared with $O(N^3)$ for a full diagonalization.

III.6. Scaling Laws of Computation. As molecular dynamics advances, the typical size of a simulation increases. As a result, calculation methods that were good for small systems become inadequate for larger ones. The knowledge of the scaling laws of computation helps to set guidelines for the appropriate strategy used to construct the simulation.

From the previous sections it can be concluded that the total computational effort is the product of the computational effort in calculating the Hamiltonian representation and the computational effort in the time propagation. Both scaling laws are proportional to the volume of phase space needed to represent the system. The total computational scaling is the product of the coordinate momentum phase-space volume and the time–energy phase-space volume. Classical trajectory calculations, being local, scale linearly with the momentum coordinate phase space. One can ask what the price of the nonlocal character of quantum mechanics on the scaling properties is. With the Fourier method as the leading example, which scales as $O(\text{Vol log (Vol)})$, the computation price of the nonlocality scales as $O(\log (\text{Vol}))$. It is conjectured that this scaling is a lower bound for the scaling properties of a nonlocal quantum-mechanical description.

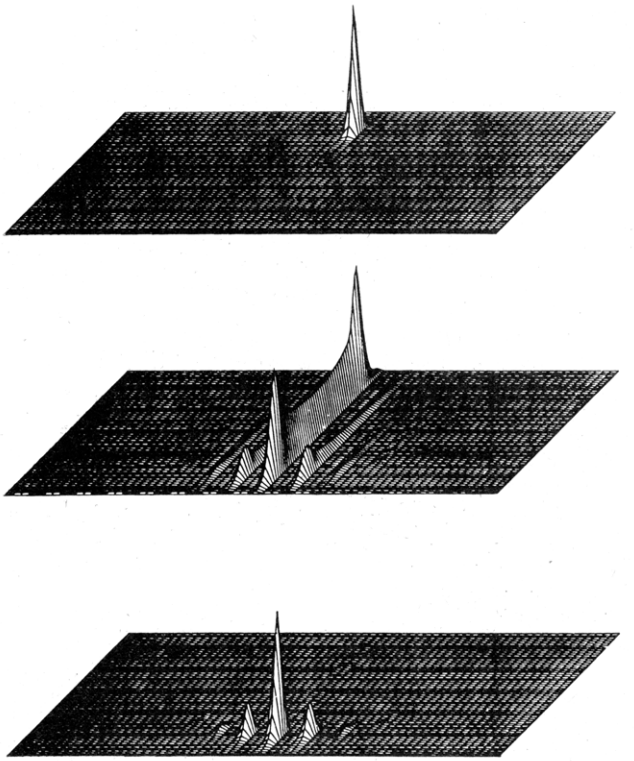

Figure 5. Snapshots of the squared amplitude of the wave function in momentum space of scattering of helium from a xenon-covered silver surface. The top figure shows the wave function at $t = 0$ with momentum directed toward the surface. The middle panel shows the wave function after $t = 15\,000$ au when the helium particle is on the surface. What can be seen is a momentum transfer from the negative direction to the positive direction. The diffraction states are also beginning to become occupied. The lower panel shows the system after the collision has been completed, $t = 30\,000$ au. The middle peak is the specular peak; the side peaks are the diffraction peaks. Up to second-order diffraction is clearly observed. (Adopted from C. Cerjan and R. Kosloff, unpublished results.)

(178) Nafha, M.; Kosloff, R., to be published.

TABLE II: Scaling Properties of Time-Dependent Methods[a]

	phase space				time–energy		convergence	
method	size	volume	number	momentum	time	energy	in space	in time
Fourier Chebychev	$L^D \log L$	Vol log Vol	$N \log N$	$P_{max}^{D+2} \log P_{max}$	t	$E^{(1/2)D+1} \log E$	exp	exp
Fourier SOD	$L^D \log L$	Vol log Vol	$N \log N$	$P_{max}^{D+3} \log P_{max}$	$t^{3/2}$	$E^{(1/2)D+3/2} \log E$	exp	power
Fourier split	$L^D \log L$	Vol log Vol	$N \log N$	$P_{max}^{D+3} \log P_{max}$	$t^{3/2}$	$E^{(1/2)D+3/2} \log E$	exp	power
finite difference	L^D	Vol	N	P_{max}^{D+3}	$t^{3/2}$	$E^{(1/2)D+3/2}$	power	power
DVR Lanczos	L^{2D}	$(\text{Vol})^2$	N^2	P_{max}^{2D}	t^2?	E^{D+2}	exp	?
diagonalization	L^{3D}	$(\text{Vol})^3$	N^3	P_{max}^{3D}	0	$E^{3D/2}$	exp	exp

[a] L is the spatial size of the box containing the system. Vol is the volume in phase space that the system occupies. N is the total number of grid points or expansion functions. P_{max} is the maximum momentum that can be represented by the descrete approximation. t is the propagation time. E is the total represented energy. D is the dimensionality of the system. Exp means exponential convergence. Power means power law convergence. The finite difference is second order in time and second order in space. The scaling laws of the Laczos method are not completely known.

It is now possible to study the influence of a few factors. First it is obvious that the coordinate extent should be minimal. Absorbing boundary conditions or adoptive grid methods are the means for this minimization. As for the momentum itself, it influences the computation in two ways—first by enlarging the coordinate momentum phase space and then by determining the energy range. For a balanced calculation between kinetic and potential energy, the energy range is proportional to the maximum momentum squared. Combining the effects, the computational effort scales with the maximum momentum as $O(P_{max}^{D+2} \log P_{max})$, where D is the dimensionality of the problem. Also, the potential energy influences the energy range so that, for a balanced calculation, a cutoff is imposed on the potential energy approximately in the same range as the maximum kinetic energy $P_{max}^2/2m$. This implies that the scaling law with respect to energy becomes $O(E_{max}^{1/2D+1} \log E_{max})$. For methods depending on a full matrix multiplication, which scale as $O(N^2)$, the total scaling laws are squared. For example, the scaling law with respect to energy becomes $O(E_{max}^{D+1})$. It should be pointed out at this point that scaling is proportional to the energy range of the problem. This means that shifting the zero of energy is equivalent to removing high frequencies and, as a result, much computational effort can be saved. With respect to time, computational effort is linear. In general, time-dependent methods are most efficient when the chemical event to be simulated has short duration. Table II summarizes the scaling properties of the common time-dependent methods.

It is speculated that, for a large and accurate simulation, the total time for a classical mechanics calculation exceeds its quantum analogue because of the more extensive sampling required in phase space. The advantage of classical mechanics is that the problem is split into many independent trajectories.

IV. Molecular Dynamics Simulation and Modeling

IV.1. As detailed experimental techniques advance, the challenge of setting up realistic simulations becomes greater. The simulated systems include many degrees of freedom, and interactions with the external fields become strong, breaking down the traditional perturbation approach. As was stated in the previous section, computational effort scales with the volume of coordinate momentum and the time–energy phase space. As a result, extensive effort should be devoted into minimizing the extent of phase space. The most fruitful scheme is to minimize the dimensionality, since computational effort scales as a power equal to the dimensionality, D. It therefore is crucial to build the simulation only around relevant coordinates and to treat the rest of the system approximately. Such an hierarchial approach is similar in spirit to the generalized Langevin framework used to treat classical mechanics in condensed phases.[34] The formal framework to exercise these ideas is the time-dependent self-consistent-field approach (TDSCF).

IV.2. The TDSCF Framework. Consider, for example, a system that can be divided into two distinct parts. The starting point of the approximation is to impose a product form on the total wave function: $\psi(x,y) \approx \phi(x)\chi(y)$. This form reduces the $n + m$ dimensional problem to a coupled n and m dimensional problem (where n is the dimensionality of the x part and m is the dimensionality of the y part). This type of approximation belongs to the family of time-dependent self-consistent-field (TDSCF) approximations.[114,115,179-185] The equations of motion are generated by inserting the product form into the Schrödinger equation (1.1)

$$i\hbar \frac{\partial \psi(x,y)}{\partial t} = i\hbar \frac{\partial \phi(x)}{\partial t} \chi(y) + i\hbar \phi(x) \frac{\partial \chi(y)}{\partial t}$$

$$= \chi(y)\hat{H}_1(x)\phi(x) + \phi(x)\hat{H}_2(y)\chi(y) + \hat{V}(x,y)\phi(x)\chi(y) \quad (4.1)$$

By multiplying by $\chi^*(y)$ and integrating on the y variable using the normalization condition $(\partial/\partial t)\langle\phi|\phi\rangle = 0$, and the fact that the right-hand side is Hermitian, the TDSCF equations are obtained:

$$i\hbar \frac{\partial \phi(x)}{\partial t} = \hat{H}_1^{SCF}(x)\phi(x) \quad (4.2)$$

and

$$i\hbar \frac{\partial \chi(y)}{\partial t} = \hat{H}_2^{SCF}(y)\chi(y)$$

where

$$\hat{H}_1^{SCF}(x) = \hat{H}_1(x) + \langle\chi(y)|\hat{H}_2(y)|\chi(y)\rangle + \langle\chi(y)|\hat{V}(x,y)|\chi(y)\rangle$$

and

$$\hat{H}_1(x) = \frac{\hat{P}_x^2}{2m} + \hat{V}(x)$$

and a similar equation for the y coordinate. The equation is solved by constructing a grid for the x and y subspaces. On this grid the operations of (4.2) are calculated. The propagation in time is carried out simultaneously in both degrees of freedom by a short-time propagator. The TDSCF scheme preserves the norm of both wave functions since $\hat{H}_{SCF}$ is Hermitian. The total energy becomes the expectation value

$$E = \langle\phi|\hat{H}_{SCF}(x)|\phi\rangle = \langle\chi|\hat{H}_{SCF}(y)|\chi\rangle \quad (4.3)$$

and is conserved in time. The advantage of the TDSCF approach is that it is very flexible in allowing different descriptions of the substituent systems while conserving the total energy.

An extreme case is a mixed quantum–classical calculation for which part of the system is treated classically and the other parts quantum mechanically. As an example, for an atom–surface encounter, the atom can be treated by using a wave function description of its state. The surface motion can be treated by using classical mechanics[101] where temperature is introduced through a generalized Langevin equation. For a low surface temperature,

(179) Dirac, P. A. M. *Proc. Cambridge Philos. Soc.* **1930**, *26*, 376.
(180) Schatz, G. C. *Chem. Phys.* **1977**, *24*, 263.
(181) Gerber, R. B.; Buch, V.; Ratner, M. A. *J. Chem. Phys.* **1982**, *77*, 3022.
(182) Gerber, R. B.; Buch, V.; Ratner, M. A. In *Intramolecular Dynamics*; Jortner, J., Pullman, B., Eds.; Reidel: Dordrecht, Holland, 1982; p 171.
(183) Kulander, K. C.; Sandhya Devi, K. R.; Koonin, S. E. *Phys. Rev. A* **1982**, *25*, 2968. Kulander, K. C. *Phys. Rev. A* **1987**, *35*, 445.
(184) Kugar, J.; Meyer, M. D.; Cederbaum, L. S. *Chem. Phys. Lett.* **1987**, *140*, 525.

the classical description has to be replaced by the density operator description of the surface motion, using the assumption that the surface phonons are harmonic,[107] and by a semigroup approach for the relaxation.[186,187] Other variations of mixed TDSCF calculations have been proposed. One that carries much promise is a quantum–semiclassical approximation using the Gaussian wave packet of Heller for the semiclassical part and a grid for the quantum part. This approximation is particularly attractive for systems that include a mixture of heavy and light particles.

When the TDSCF approximation is used, the problem of omitted correlations has to be addressed. Unlike static SCF, which leaves out all correlations, in the time-dependent SCF, part of the correlations are taken into consideration by the time evolution. The TDSCF method allows flow of energy from one mode to the other subject to total energy conservation. Nevertheless, important correlations may still be left out. This can be corrected systematically by adding configurations, producing a *m*ulticonfiguration *t*ime-*d*ependent *s*elf-*c*onsistent-*f*ield (MC-TDSCF) description. This possibility has only barely been explored.[114,185] The main impetus behind multiconfiguration is to allow more flexibility in the wave function, thus allowing the incorporation of correlations. The idea is to include in the calculation only the physically relevant correlations. As an illustration, the simple wave function that is a sum of products in the x and y space is considered:

$$\psi(x,y) = \phi_1(x)\chi_1(y) + \phi_2(x)\chi_2(y) \tag{4.4}$$

Normalization is imposed on the x space. The correlations are introduced subject to the projection operator which is defined in the y space.

$$\hat{P}(y)\chi_1(y) = \chi_1(y)$$
$$\hat{P}(y)\chi_2(y) = 0 \tag{4.5}$$

The choice of the projection operator determines the correlation. For example, the projection operator can differentiate between reactive and nonreactive channels. Imposing total normalization, $\langle\psi|\psi\rangle = 1$, one obtains in the y space

$$\langle\chi_1|\chi_1\rangle + \langle\chi_2|\chi_2\rangle = 1 \tag{4.6}$$

This leads to the interpretation of the amplitude $\langle\chi_i|\chi_i\rangle$ as the probability associated with the projection $\hat{P}$. Inserting (4.4) into the Schrödinger equation (1.1) and imposing the normalization conditions, the MC-TDSCF equations are obtained:

$$i\hbar\frac{\partial\chi_1}{\partial t} = [\langle\phi_1|\hat{H}_x|\phi_1\rangle + \hat{P}\hat{H}_y + \hat{P}\langle\phi_1|\hat{V}_{xy}|\phi_1\rangle]\chi_1 + [\hat{P}\hat{H}_y\langle\phi_1|\phi_2\rangle + \hat{P}\langle\phi_1|\hat{V}_{xy}|\phi_2\rangle]\chi_2$$

$$i\hbar\frac{\partial\phi_1}{\partial t} = \left[-i\frac{\langle\chi_1|\dot{\chi}_1\rangle}{\langle\chi_1|\chi_1\rangle} + \hat{H}_x + \frac{\langle\chi_1|\hat{H}_y|\chi_1\rangle}{\langle\chi_1|\chi_1\rangle} + \frac{\langle\chi_1|\hat{V}_{xy}|\chi_1\rangle}{\langle\chi_1|\chi_1\rangle}\right]\phi_1 + \left[\frac{\langle\chi_1|\hat{H}_y|\chi_2\rangle}{\langle\chi_1|\chi_1\rangle} + \frac{\langle\chi_1|\hat{V}_{xy}|\chi_2\rangle}{\langle\chi_1|\chi_1\rangle}\right]\phi_2 \tag{4.7}$$

In a similar fashion the equations of motion for ϕ_2 and χ_2 are obtained. The choice of the projection $\hat{P}$ is where physical intuition takes place.

The quality of the TDSCF and the MC-TDSCF approximation very much depends on the choice of coordinates. This choice can be led by physical intuition, looking for a natural separability such as that arising from different time scales or mass differences. A more systematic approach is to optimize the coordinates. For static SCF this has been carried out successfully with a variational approach.[188] For TDSCF an approach based on the time-dependent variational procedure has been suggested.[184] In this method the representation in phase space is optimized continuously in time. A similar idea may apply to MC-TDSCF where the projection operator $\hat{P}$ defining the correlation will be optimized continuously in time.

IV.3. Applications. Time-dependent quantum-mechanical calculations have just begun to proliferate so that most applications are in an initial stage. Nevertheless, in several fields of research, time-dependent quantum-mechanical methods have caused a significant impact. In computational physics, existing working codes have developed "momentum". The new methods have entered areas in which there has been no known alternative or they have shown significant increase in efficiency. Because of their scaling properties, time-dependent approaches become more attractive when phase space is large. For problems requiring thousands of channels, they gain in importance because the traditional coupled channel methods are inadequate. Another example of a problem for which time-dependent methods have no feasible alternative is a system that includes more than one continuum of states. This situation occurs in a collision-induced or laser-induced dissociation. One of the most important reasons for using these methods is the insight that can be gained by inspecting intermediate results, unique to the time-dependent approach.

Atomic and molecular surface encounters is an area where time-dependent calculations have contributed significantly. The main reason has been the easy implementation of the Fourier method to a basically Cartesian coordinate system, where the periodic boundary conditions can be matched to the surface unit cell. The calculations performed can be divided into ones with static or a dynamic description of the surface. Static calculations concentrate on problems related to surface structure. Many of these are very large scattering problems, which make time-dependent methods attractive. For example, in the work of Yinnon et al.,[96-98] time-dependent calculations have been used to elucidate the physical phenomena associated with single impurities and isolated vacancies on metal surfaces. Another calculation[102] has been concerned with scattering from disordered surfaces. Three-dimensional calculations including up to 4096 diffraction channels were performed regularly. Molecular surface scattering calculations are concerned with interaction of the molecular degrees of freedom with the surface. The problem is six dimensional, making it a computational challenge. Current calculations concentrate on rotational excitation, elucidating the connection between rotational excitation and the diffraction pattern. The systems studied include H_2, D_2, and N_2 rotational excitation.[122-126] The very large number of asymptotic scattering channels has led to the largest scattering calculation to date, which was performed for the scattering of N_2 from a surface displaying rotational rainbows.[126]

Dynamical surface calculations are aimed at understanding inelastic and energy-transfer phenomena between the gas molecule and the surface, The time dependence is used explicitly to include the continuum of phonon states. Calculations have been carried out for desorption energy accommodation and phonon excitation. The general framework of these calculations is a TDSCF approach in which the surface motion and the molecular motion are separated. In this framework, surface motion can be treated either classically for high surface temperature or quantum mechanically for low surface temperature. Molecular dissociation dynamics on a surface is a field in which time-dependent calculations will contribute significantly. The objective is to understand the detailed dynamics of the first stage in homogeneous surface catalysis.[134] A review of time-dependent quantum-mechanical methods in surface scattering has appeared recently.[108]

Photochemical processes is a field in which time-dependent calculations are expected to have great impact. As was described in section III, time-dependent methods lend themselves to the calculation of spectra.[117,141] In particular, the method has sig-

(185) Makri, N.; Miller, W. H. *J. Chem. Phys.* **1987**, *87*, 5781.
(186) Lindblad, G. *Commun. Math. Phys.* **1976**, *48*, 119.
(187) Gorini, V.; Kossakowski, A.; Sudarshan, E. C. G. *J. Math. Phys.* **1976**, *17*, 821.
(188) Bacic, Z.; Gerber, R. B.; Ratner, M. A. *J. Phys. Chem.* **1986**, *90*, 3606.
(189) Luk, T. S.; Johann, U.; Egger, H.; Pummer, H.; Rhods, C. K. *Phys. Rev. A* **1985**, *32*, 214.

nificant advantages when the spectra are of molecules undergoing photodissociation. The method is particularly efficient for fast processes in the femtosecond region requiring short integration times. One such example has been to prove the feasibility of photoselective processes by using a pulsed sequence of light.[110]

A similar idea was used to describe the ionization dynamics of atoms and molecules in very intense laser fields.[189] The purpose of the calculation was to obtain the photoionization rate far beyond the fields that can be described by perturbation theory.[112] In this calculation the time dependence was used explicitly to describe the electromagnetic field as a time-dependent vector potential: $\hat{T} = (\hat{P} - e/c\hat{A}(t))^2/2m$.

Time-dependent methods have many advantages in the study of molecular mechanisms. The ability to review snapshots of the wave function in intermediate stages of the process facilitates identification of a molecular mechanism. Studies on these lines have been devoted to the process of resonance decay. The systems studied include the dissociation dynamics of the collinear van der Waals complex of HeI_2.[115,129] This study was carried out by both an exact time-dependent method and the TDSCF approximation. Detailed studies on the dissociation dynamics of the model collinear kinetically coupled Morse oscillators have shown a great variety of dissociation lifetimes for resonances with almost the same energy.[103-105,191]

Reactive scattering problems are the slowest to have been developed. Many collinear reactions have been studied with the main advantage of gaining insight into the detailed dynamics. The systems studied include $H + H_2$, F + DBr, $H^+ + H_2$,[95] and more. Also, collision-induced-dissociation calculations were performed. Here the time-dependent method was chosen because of its ability to treat multiple continua.[87-90] Almost all time-dependent calculations are restricted to collinear geometry. The reason is the complexity of the coordinate system for a total J conservation. The resulting curvilinear coordinates are not simply represented by the Fourier method, and other collocation methods have still to be developed. It may be desirable to simulate these reactive systems in six-dimensional Cartesian coordinates. The simplicity will compensate for the saving due to the conservation of total angular momentum.

The latest topic is the simulation of electrons in condensed phases. The framework is a TDSCF quantum–classical calculation where the dynamics of the nuclear motion is treated classically. Calculations were applied to an electron in a cluster[146] and to electrons in molten salts.[142,143] Advances have been also made in the treatment of electronic motion by static SCF calculations using pseudospectral methods.[191]

Projecting to new applications, methods scaling as the Fourier method will play a dominant role. As the simulated problem becomes larger, the slower scaling methods become more and more attractive. The Fourier method, while allowing very high accuracy because it describes correctly the nonlocal character of quantum mechanics, has the slowest scaling properties.

(190) Bisseling, R. H.; Gertitschke, P. L.; Kosloff, R.; Manz, J. *J. Chem. Phys.*, in press.
(191) Friesner, R. A. *J. Chem. Phys.* **1987**, *86*, 3522.

V. The Future

In developing today's algorithms, it is important to foresee tomorrow's applications and the hardware tools that will be available. This is in order to incorporate as many as possible future requirements in the present algorithms, whose lifetime might well extend into the next computer generation.

The rule of thumb of computer architects is that every five years a new computer generation is born, with computing power enlarged by an order of magnitude. Since computational effort scales as the volume in phase space, this implies that the frontier of solvable problems is pushed one dimension forward every seven or eight years. The current status is that, on fast minicomputers, three-dimensional molecular problems can be performed and, on supercomputers, four-dimensional problems can be performed. For electrons, which are lighter, the current status is that six-dimensional calculations can be performed. From this the conclusion can readily be drawn that, even with fast development of new computers, the frontier continues to move very slowly. This points to the importance of developing good approximation methods, instead of waiting until the year 2000, for solving a six-dimensional reactive scattering problem. The same problem can be solved today by appropriately separating out two subspaces by using the TDSCF method. The benchmark function of accurate time-dependent methods is a help in gaining physical insight into how valuable the approximation technique is.

Besides the trend of faster machines with larger memory, there is another trend that can be noticed today, which is the development of parallel machines. Since there is a limit to how fast a single processor can work, the obvious way to expand computing power is to connect many of them into a parallel machine.

Algorithms that can be parallelizable might survive into the next computer generation, while others that cannot might perish. Consequently, algorithms that are inferior on sequential machines might be the superior ones on parallel machines. This fact necessitates a reevaluation of existing algorithms, in consideration of the development of parallel new algorithms. The Fourier method is highly parallelizable, since FFT's are. The TDSCF method can be implemented in parallel in a natural way and because of this might gain prominence.

In conclusion, the combination of collocation methods highly gained by parallelizable approximation algorithms might be the right way to confront high-dimensional molecular dynamics problems in the future. Time-dependent quantum-mechanical methods will play a major role in future simulations because of their accuracy, flexibility, and efficiency leading to greater insight into dynamical molecular processes.

Acknowledgment. I thank my collaborators, A. D. Hammerich, R. Bisseling, C. Cerjan, B. Gerber, M. Ratner, T. Yinnon, J. Manz, C. LeForestier, M. Berman, H. Tal-Ezer, and D. Kosloff for many contributions and J. C. Light, A. Halperin, and R. D. Levine for helpful discussions. Work supported by the United States–Israel Binational Foundation. The Fritz Haber Research Center is supported by the Minerva Gesellschaft für die Forschung, GmbH München, BRD.